CHAPTER V

RESULTS AND DISCUSSION

5.1 Synthesis of ligands and iron complexes

5.1.1 $RHN(CH_2)_3NHR$ (R = $2,6^{i}Pr_2C_6H_3$) ligand (**a**)

The synthesis of 1,3-di(2,6-diisopropylphenyl)aminopropane was as follows:

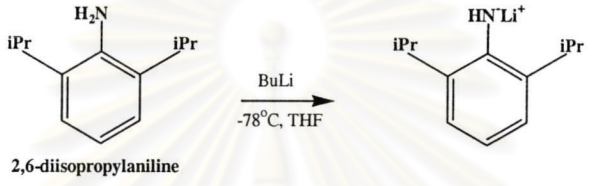

2,6-diisopropylaniline

(10)

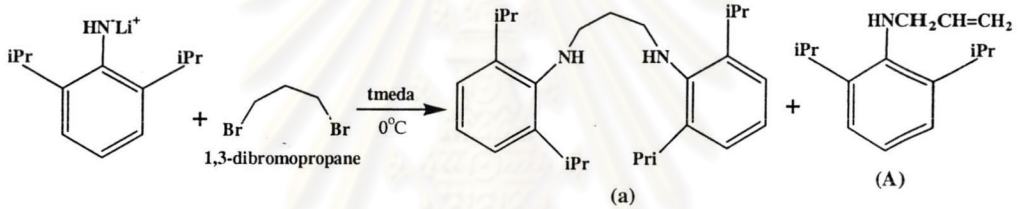

1,3-dibromopropane

(a)

(A)

(11)

The 1,3-di(2,6-diisopropylphenyl)aminopropane; ligand (**a**) was prepared from the reaction between 2,6-diisopropylaniline and 1,3-dibromopropane. 2,6-Diisopropylaniline was firstly lithiated with BuLi at –78°C to afford LiNHR (R = 2,6-$^{i}Pr_2C_6H_3$). The diamine ligand (**a**) was obtained from the reaction of two equivalents of LiNHR with 1,3-dibromopropane at 0°C. This ligand had been used to react with $TiCl_4$ to synthesize titanium complex which was found a good catalyst for 1-hexene polymerization when activated with boron cocatalyst.[50]

The ligand (**a**) was formed together with the elimination product $RHNCH_2CH{=}CH_2$ (**A**) in a 1:1 ratio. The facile formation of byproduct **A** necessitates the use of tetramethylethylenediamine (tmeda) since reaction performed without tmeda contained about 80% of byproduct **A**.[50] The possible mechanism of tmeda during the formation of ligand (**a**) was shown in Scheme 5.1. The diamine ligand (**a**) as orange oil (88% yield) was separated from **A** via purification using silica gel column chromatography and dichloromethane:hexane (7:3) as eluent.

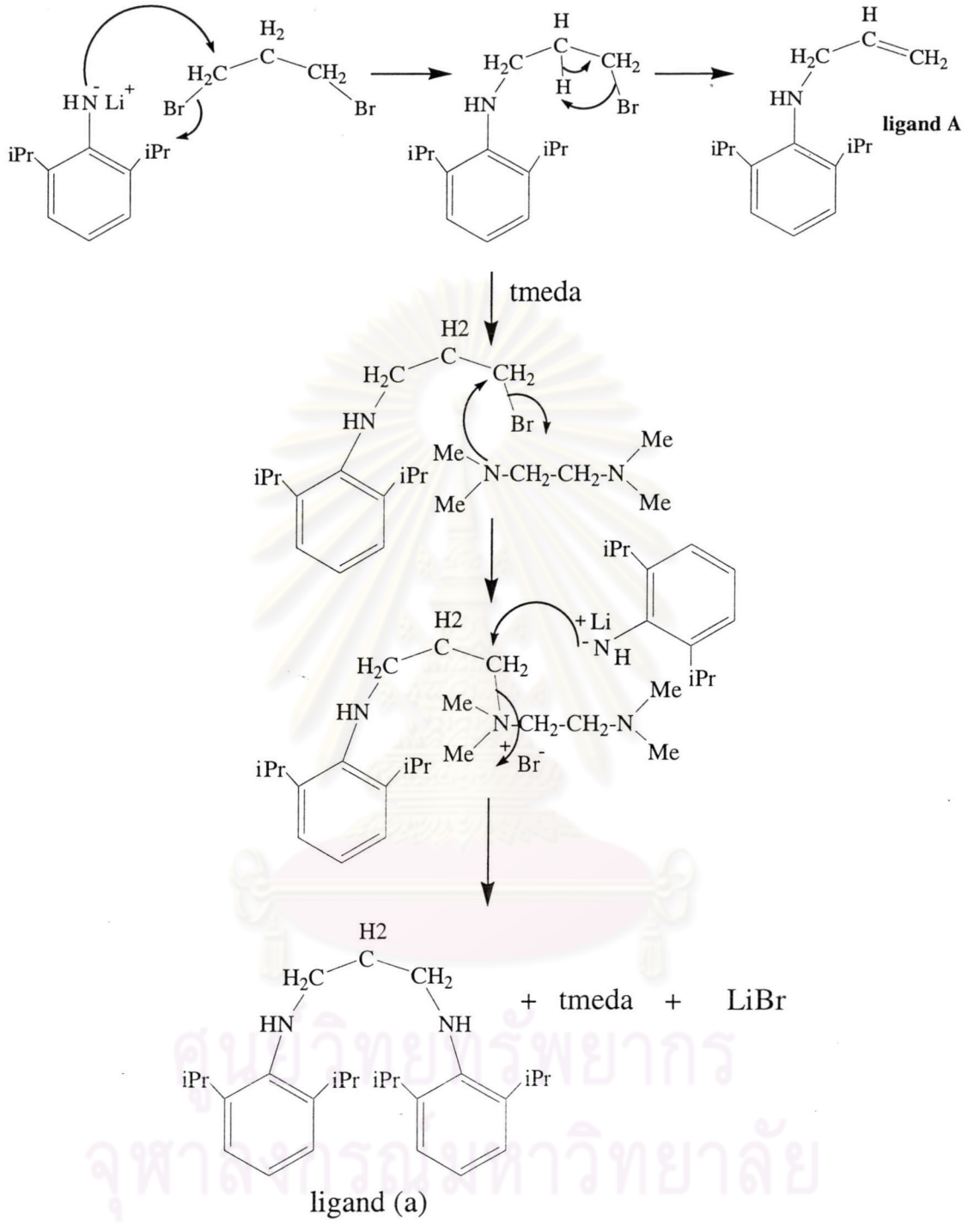

Scheme 5.1 Possible mechanism of tmeda during ligand (**a**) synthesis.

^{1}H-NMR, ^{13}C-NMR spectra, FT-IR spectrum and UV-visible spectrum of ligand (**a**) were shown in Figures 5.1-5.4. The assignments of peaks are in Tables 5.1-5.3.

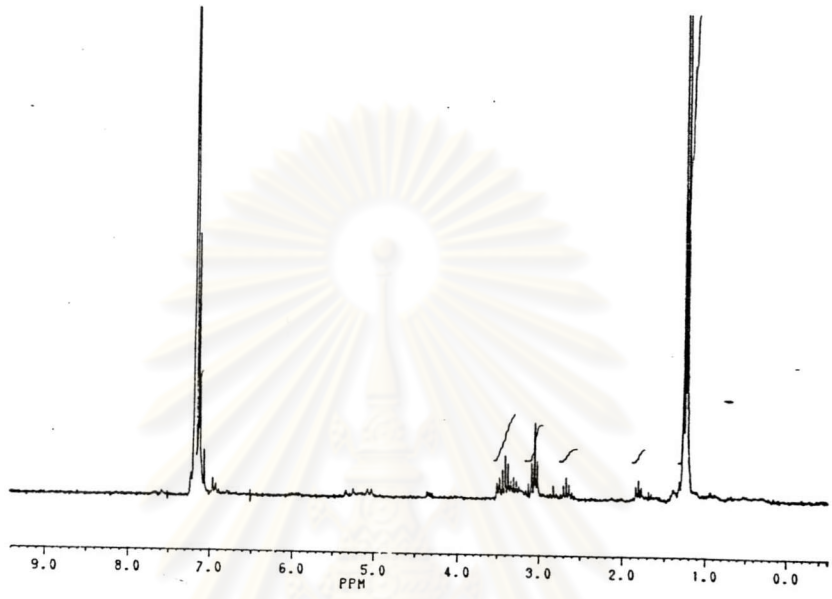

Figure 5.1 ^{1}H-NMR (C_6D_6) spectrum of ligand (**a**).

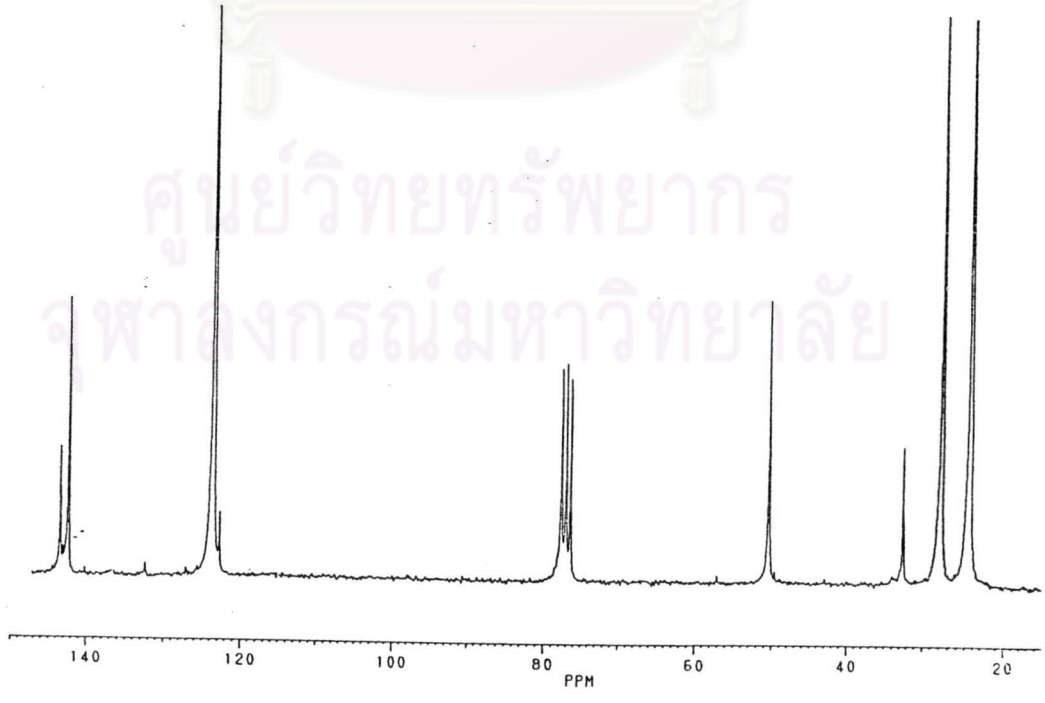

Figure 5.2 ^{13}C-NMR (C_6D_6) spectrum of ligand (**a**).

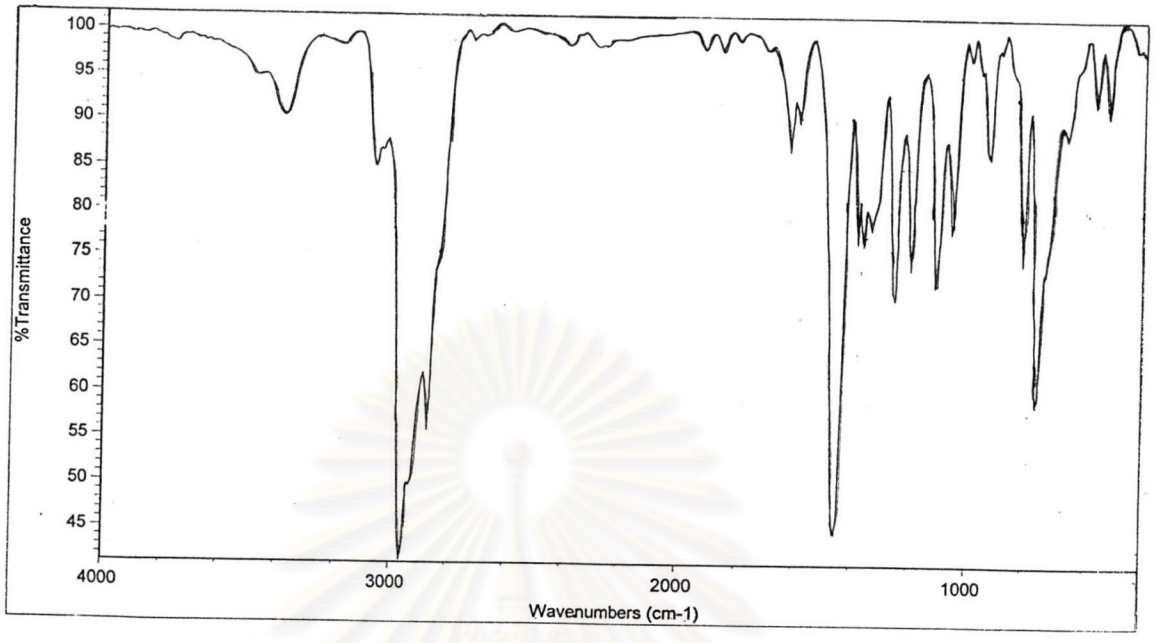

Figure 5.3 FT-IR spectrum of ligand (**a**).

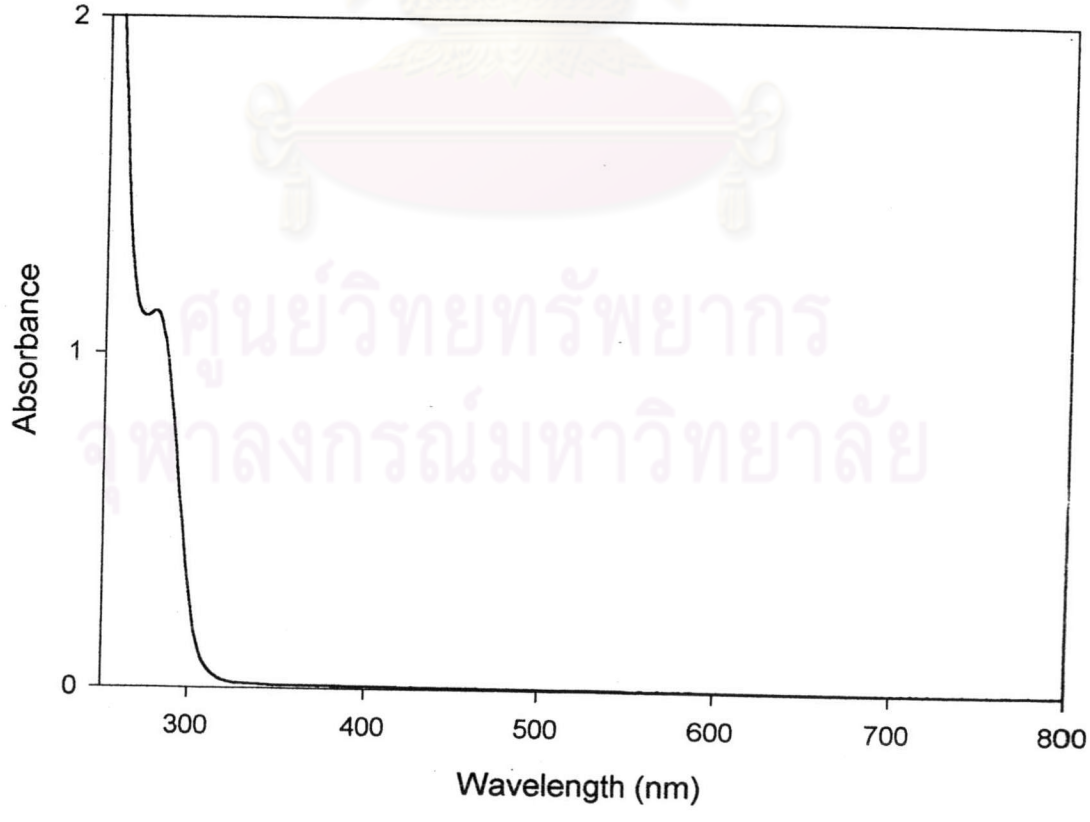

Figure 5.4 UV-visible spectrum of ligand (**a**).

Table 5.1. ^{1}H-NMR data of the ligand (**a**)

Chemical shift (ppm)	Multiplicity	Number of protons	Assignment
7.12	multiplet	6H	C_6H_3
3.37	septet	4H	$CHMe_2$ (J = 6.9Hz)
3.02	triplet	4H	NCH_2 (J = 6.9 Hz)
2.97	triplet	2H	NH (J = 6.9 Hz)
1.77	triplet	2H	NCH_2CH_2 (J = 6.9 Hz)
1.26	doublet	24H	$CHMe_2$ (J = 6.8 Hz)

The ^{1}H-NMR of ligand (**a**) showed a multiplet peak at 7.12 ppm that is assigned to aromatic ring protons. Two triplet peaks at 3.02 and 1.77 ppm are assigned to propyl protons. Septet peak at 3.37 and doublet peak at 1.26 ppm are assigned to substituted propyl protons on aromatic ring. The triplet peak at 2.97 ppm is assigned to amine protons.

Table 5.2. ^{13}C-NMR data of the ligand (**a**)

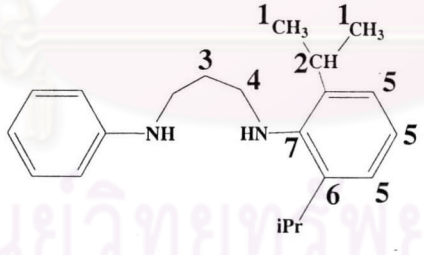

Chemical shift (ppm)	Assignment
143.5	C^7
142.4	C^6
123.6	C^5
50.3	C^4
32.4	C^3
27.8	C^2
24.4	C^1

Table 5.3. FT-IR data of ligand (**a**)

Wave number (cm^{-1})	Assignment
3371	N-H stretching
3050	C-H aromatic stretching
2950	$-CH_3$ stretching
2865	$-CH_2$ stretching
1621	C=C stretching
1451, 1362	$-CH_2$, $-CH_3$ bending
1254	C-N stretching

The ^{13}C-NMR of ligand (**a**) consisted of aromatic ring carbons at 143.5, 142.4 and 123.6 ppm, propyl carbons between two amine groups at 50.3 and 32.4 ppm and substituted isopropyl carbons on aromatic ring at 27.8 and 22.4 ppm. FT-IR spectrum showed N-H stretching peak at 3371 cm^{-1}, strong sharp peak of C-H stretching at 3050 and 2950 cm^{-1} and medium peak of C-N stretching at 1254 cm^{-1}. The UV-visible spectrum of ligand (**a**) showed λ_{max} at 279 nm that is an absorption of aromatic ring Π-bond.

5.1.2 $[RHN(CH_2)_3NHR]FeCl_3$ (R = 2,6-$^{i}PrC_6H_3$) complex, **cpx 1a**

The synthesis of **cpx 1a** was as follows:

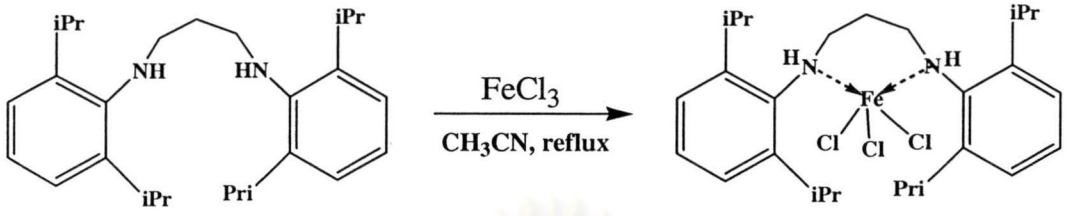

(12)

cpx 1a

The reaction of the diamine ligand (**a**) with $FeCl_3$ in refluxing acetonitrile afforded the iron complex, $[RHN(CH_2)_3NHR]FeCl_3$ (R = 2,6-$^{i}PrC_6H_3$) (**cpx 1a**) as dark red solids (36% yield). Molecular formula of **cpx 1a** calculated from elemental analysis is $C_{27}H_{42}N_2FeCl_3$. This means that one equivalent of $FeCl_3$ reacted with one equivalent of ligand (**a**).

The FT-IR spectrum of the **cpx 1a** showed broad peak of N-H stretching at 3409 cm^{-1}. This means that hydrogen at the amine group in ligand (**a**) was not abstracted when the ligand was reacted with $FeCl_3$. This iron complex showed absorption bands in UV-visible spectrum at λ_{max} 491 and 551 nm. Since the **cpx 1a** is paramagnetic therefore it exhibited broad ^{1}H-NMR spectrum.

The FT-IR spectrum, UV-visible spectrum and the FT-IR assignment of peak of **cpx 1a** were shown in Figures 5.5-5.6 and Table 5.4 respectively.

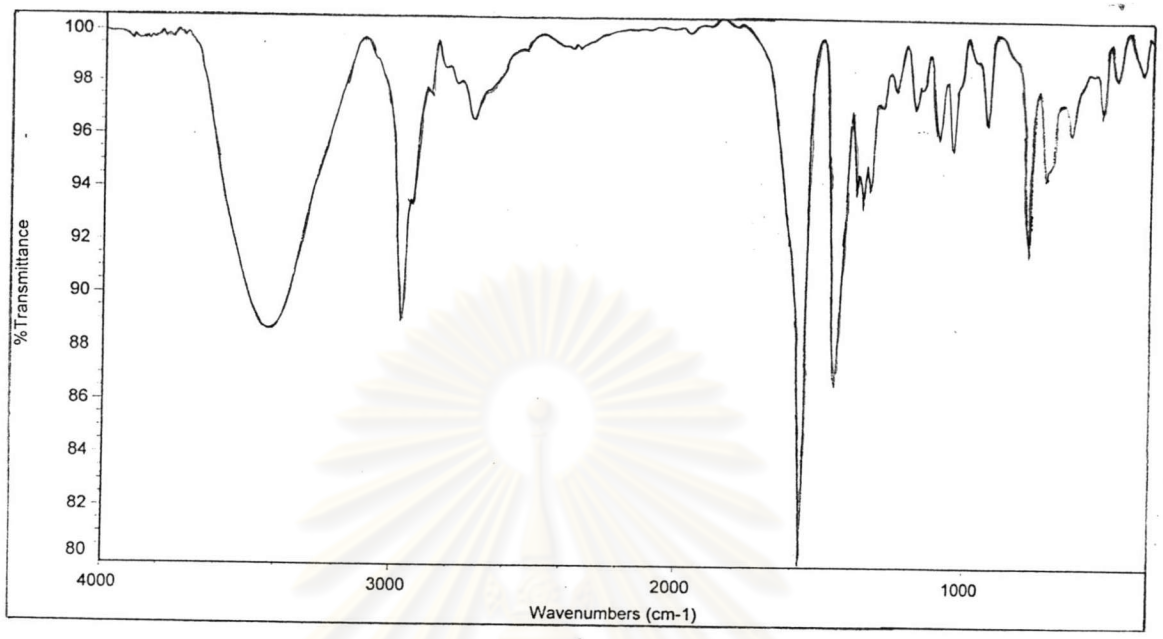

Figure 5.5 FT-IR spectrum of **cpx 1a**.

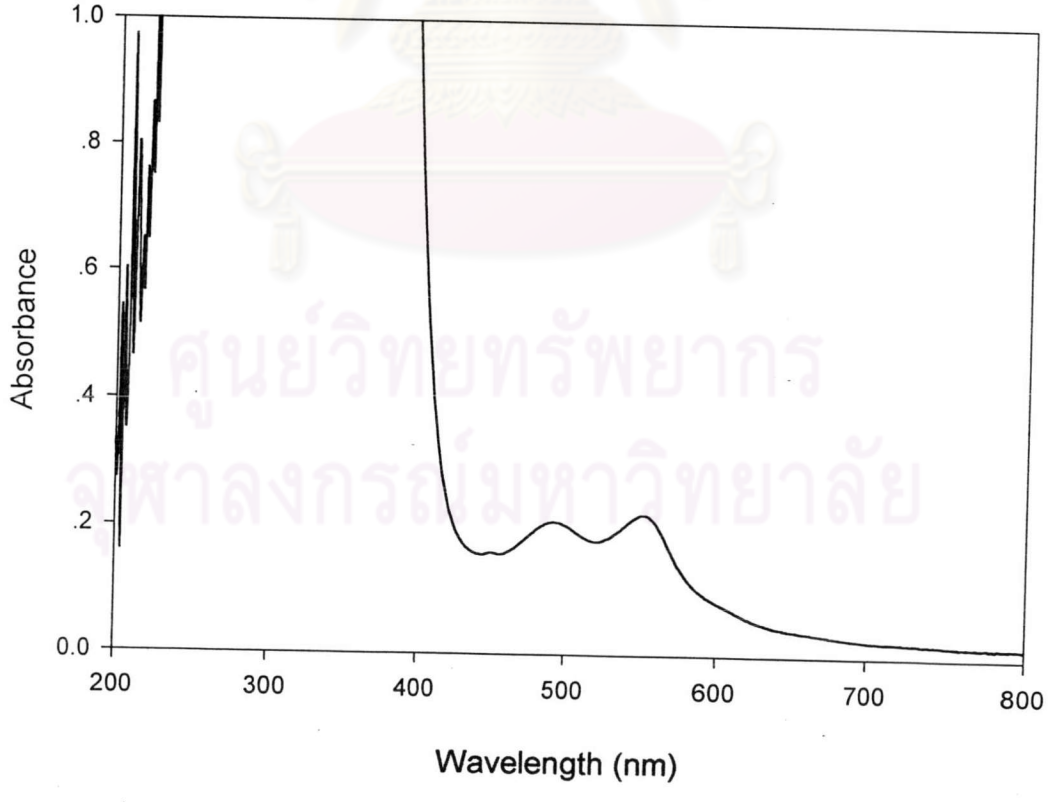

Figure 5.6 UV-visible spectrum of **cpx 1a**.

Table 5.4. FT-IR data of **cpx 1a**

Wave number (cm^{-1})	Assignment
3409	N-H stretching
2968	C-H aliphatic stretching
1574	C=C stretching
1461, 1367	$-CH_2$, $-CH_3$ stretching

5.1.3 $RHN(CH_3)C=C(CH_3)C=NR$ (R = $2,6^iPr_2C_6H_3$) ligand (**b**)

The synthesis of 1-((2,6-diisopropylphenyl)amino)-4-((2,6-diisopropyl phenyl) imino)-2-pentene, ligand (**b**) was as follows:

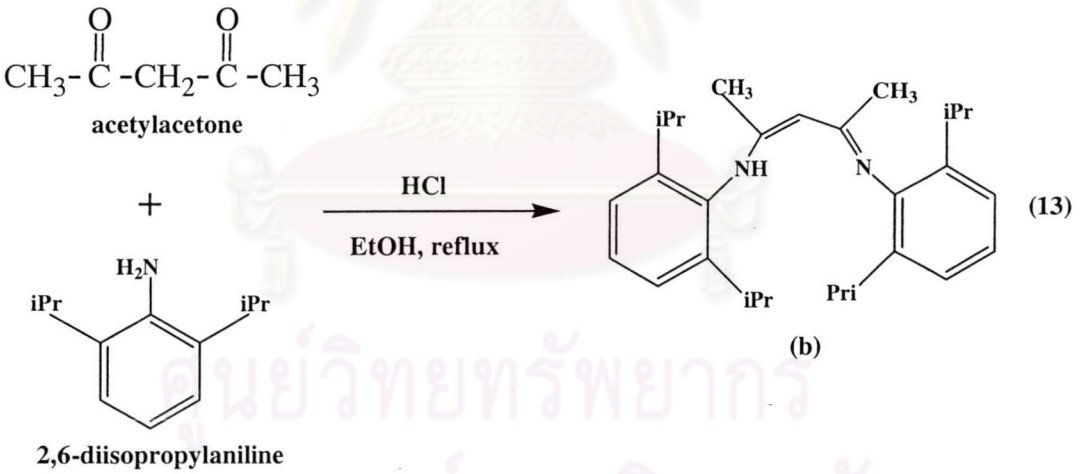

The imine ligand (**b**) as white crystalline solids (46 %yield) was prepared from the condensation of two equivalents of 2,6-diisopropylaniline with one equivalent of acetylacetone. Hydrochloric acid was added as catalyst in the reaction. This ligand had been used for synthesis of chromium chloride complexes which could polymerize ethylene. The activity in ethylene polymerization was moderate.[58,60]

^{1}H-NMR spectrum, FT-IR spectrum and UV-visible spectrum of ligand (**b**) were shown in Figures 5.7-5.9. The assignments of peaks are in Tables 5.5-5.6.

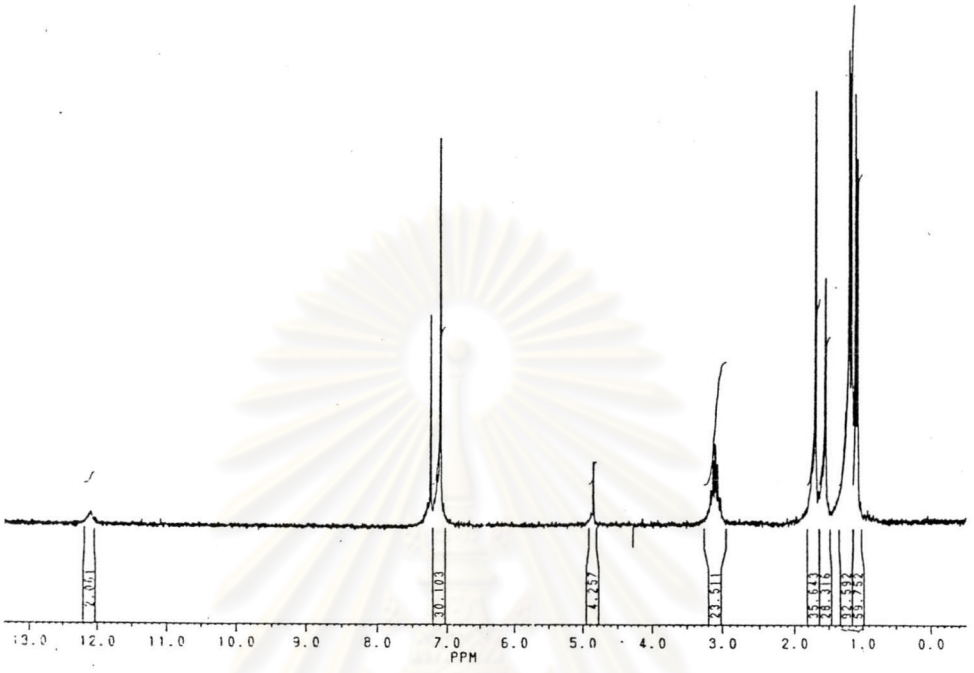

Figure 5.7 ^{1}H-NMR ($CDCl_3$) spectrum of ligand (**b**).

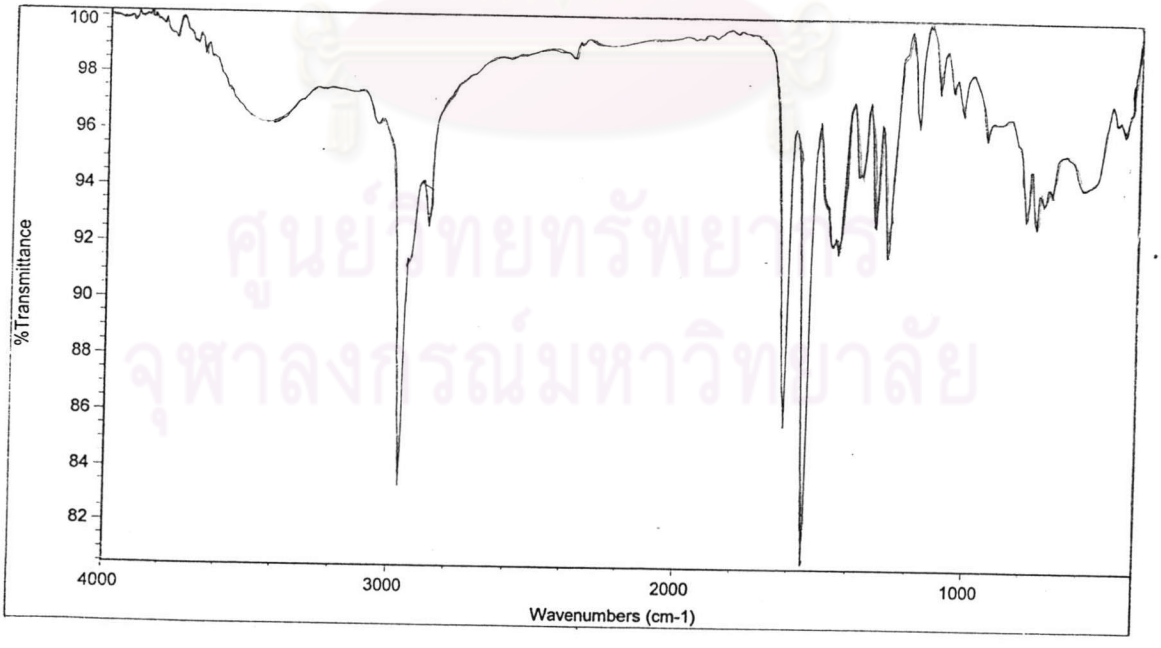

Figure 5.8 FT-IR spectrum of ligand (**b**).

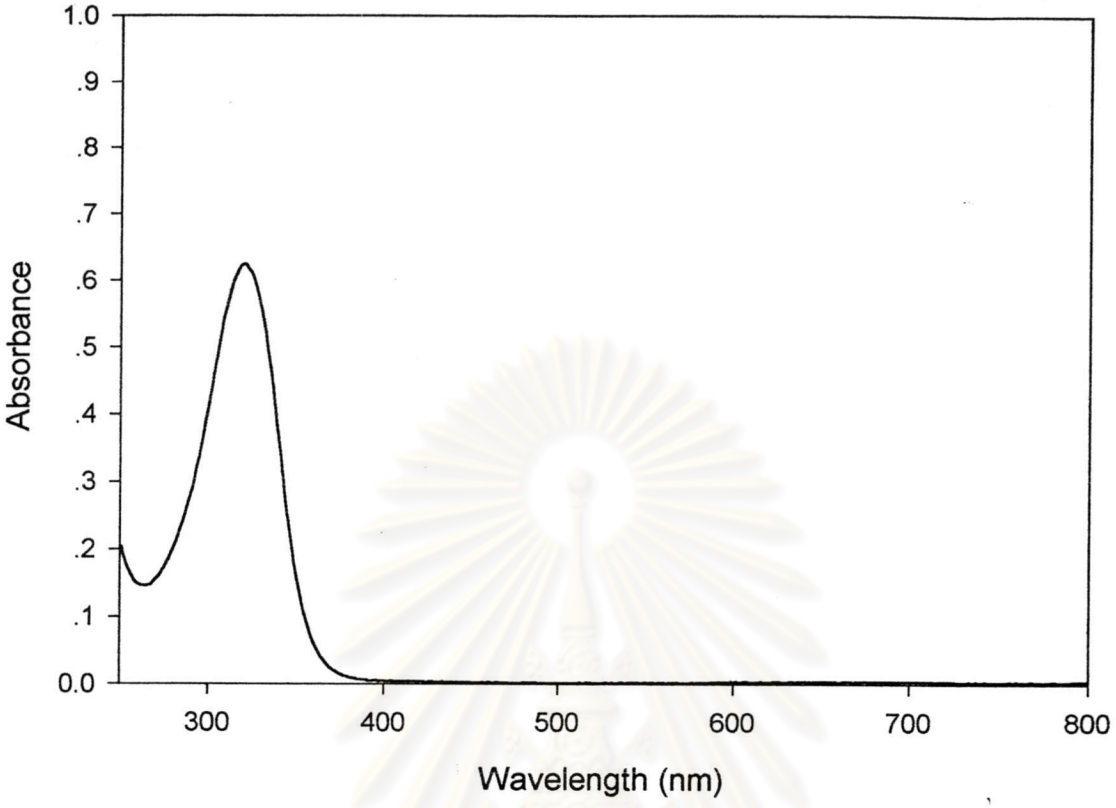

Figure 5.9 UV-visible spectrum of ligand (**b**).

Table 5.5. ^{1}H-NMR data of ligand (**b**)

Chemical shift (ppm)	Multiplicity	Number of protons	Assignment
12.09	broad	1H	N*H*
7.10	multiplet	6H	H_{aryl}
4.84	singlet	1H	H_{β}
3.09	multiplet	4H	C*H*Me$_2$
1.69	singlet	3H	α-Me
1.55	singlet	3H	α-Me
1.20	doublet	12H	CH*Me*$_2$ (J = 6.8 Hz)
1.12	doublet	12H	CH*Me*$_2$ (J = 6.9 Hz)

The ^{1}H-NMR of ligand (**b**) can be assigned as follows; a broad peak at 12.09 ppm is assigned to amine proton. A multiplet peak at 7.10 ppm is assigned to aromatic ring protons. A singlet peak at 4.84 ppm is assigned to β-proton at propene chain. Singlet peaks at 1.69 and 1.55 ppm are assigned to α-methyl group at propene chain. A multiplet peak at 3.09 ppm and two doublet peaks at 1.20 and 1.12 ppm are assigned to isopropyl on aromatic ring.

Table 5.6. FT-IR data of ligand (**b**)

Wave number (cm^{-1})	Assignment
3381	N-H stretching
2959	$-CH_3$ stretching
2880	$-CH_2$ stretching
1621	C=C stretching
1442, 1376	$-CH_2$, $-CH_3$ bending
1277	C-N stretching

FT-IR spectrum showed broad peak of N-H stretching at 3381 cm^{-1}, strong sharp peak of C-H stretching at 2959 cm^{-1} and medium peak of C-N stretching at 1277 cm^{-1}. The ligand (**b**) showed the UV-visible absorption from aromatic Π-bond at λ_{max} 320 nm.

5.1.4 [RHN(CH_3)C=C(CH_3)C=NR]$FeCl_3$ (R = 2,6-$^{i}PrC_6H_3$) complex, **cpx 2b**

The synthesis of **cpx 2b** was as follows:

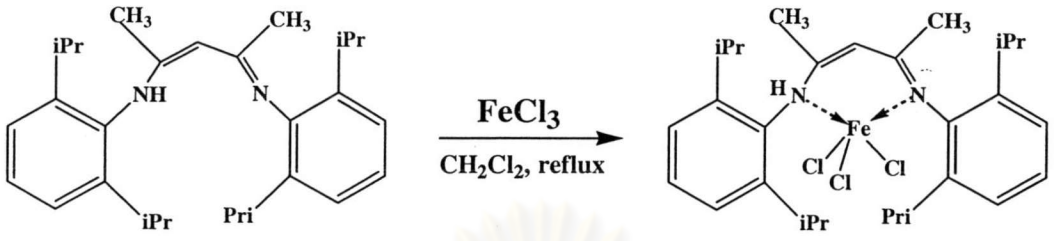

(14)

cpx 2b

The direct treatment of one equivalent of $FeCl_3$ with one equivalent of imine ligand (**b**) in refluxing dichloromethane afforded the iron complex, [RHN(CH_3)C=C(CH_3)C=NR]$FeCl_3$ (R = 2,6-$^{i}PrC_6H_3$) (**cpx 2b**) as orange solid (26 %yield). Calculation from elemental analysis showed that molecular formula of **cpx 2b** is $C_{29}H_{42}N_2FeCl_3.CH_2Cl_2$.

The FT-IR spectrum of the **cpx 2b** in Figure 5.10 showed broad peak of N-H stretching at 3428 cm^{-1}. This means that hydrogen at the amine group in ligand (**b**) was not abstracted when the ligand was reacted with $FeCl_3$. The iron **cpx 2b** showed new absorption bands of the UV-visible spectrum at λ_{max} 466 and 626 nm.

The FT-IR spectrum, UV-visible spectrum and the FT-IR assignment of peak of this complex were shown in Figures 5.10-5.11 and Table 5.7 respectively.

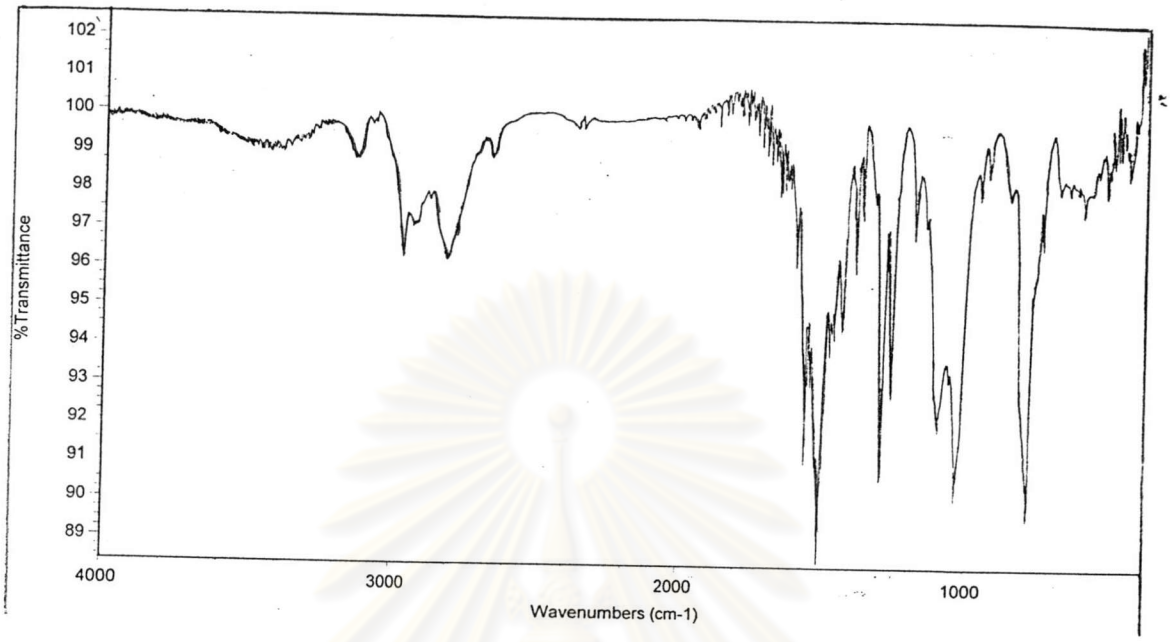

Figure 5.10 FT-IR spectrum of **cpx 2b**.

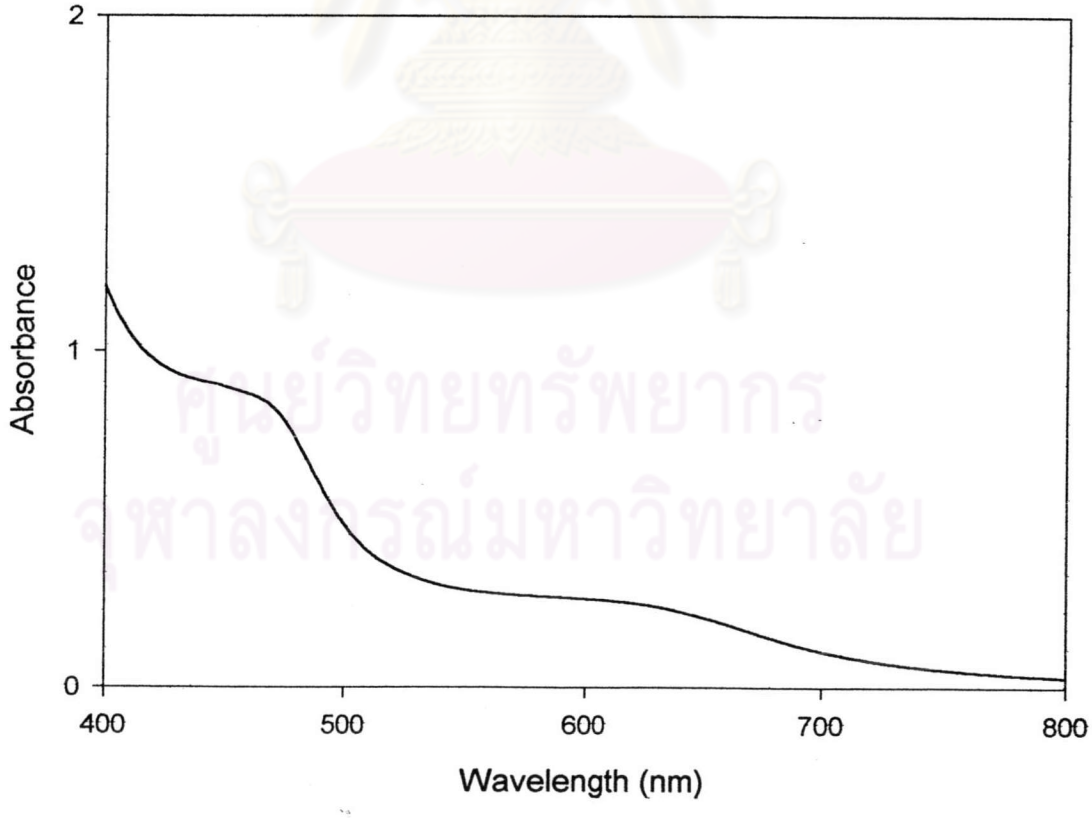

Figure 5.11 UV-visible spectrum of **cpx 2b**.

Table 5.7. FT-IR data of **cpx 2b**

Wave number (cm^{-1})	Assignment
3428	N-H stretching
2970	$-CH_3$ stretching
2809	$-CH_2$ stretching
1503	C=C stretching
1428	$-CH_2$, $-CH_3$ bending
1296	C-N stretching

5.1.5 Bis(salicylaldehyde)ethylenediimine (salen), ligand (**c**)

The synthesis of salen was as follows:

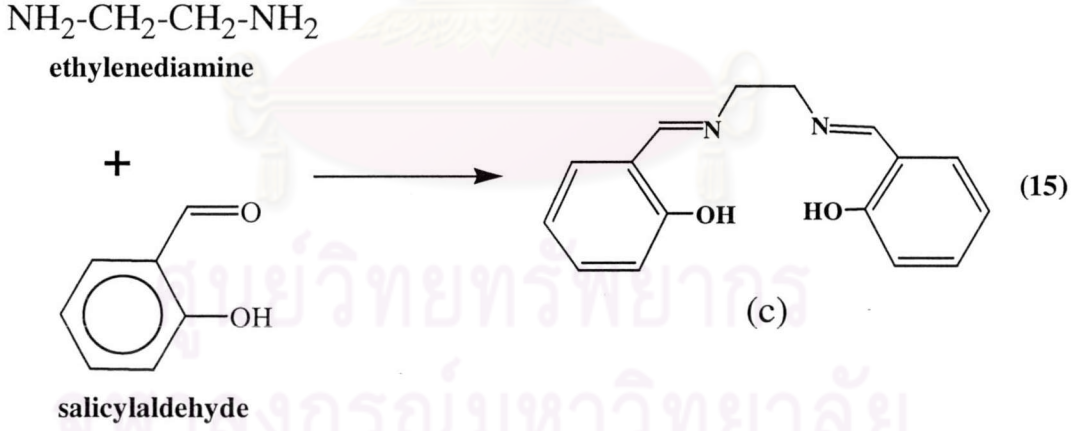

The Schiff base ligand (**c**) was synthesized in high yield (97 %yield) by condensation reaction between one equivalent of ethylenediamine and two equivalents of salicylaldehyde. Ligand (**c**) as yellow crystal was immediately occurred after the reaction was heated.

^{1}H-NMR spectrum, FT-IR spectrum and UV-visible spectrum of ligand (**c**) were shown in Figures 5.12-5.14. The assignments of peaks are in Tables 5.8-5.9.

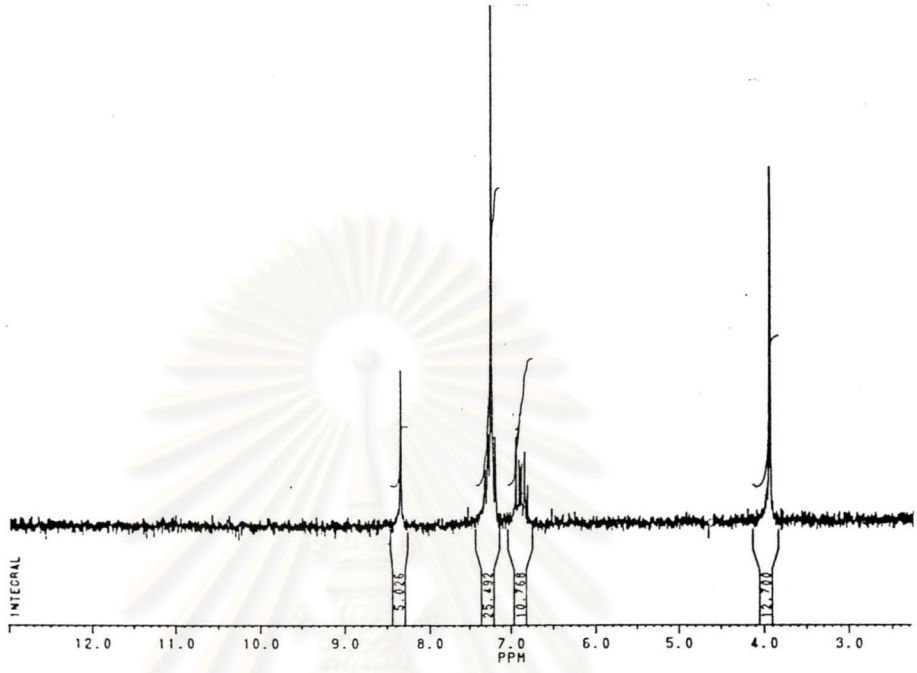

Figure 5.12 ^{1}H-NMR ($CDCl_3$) spectrum of ligand (**c**).

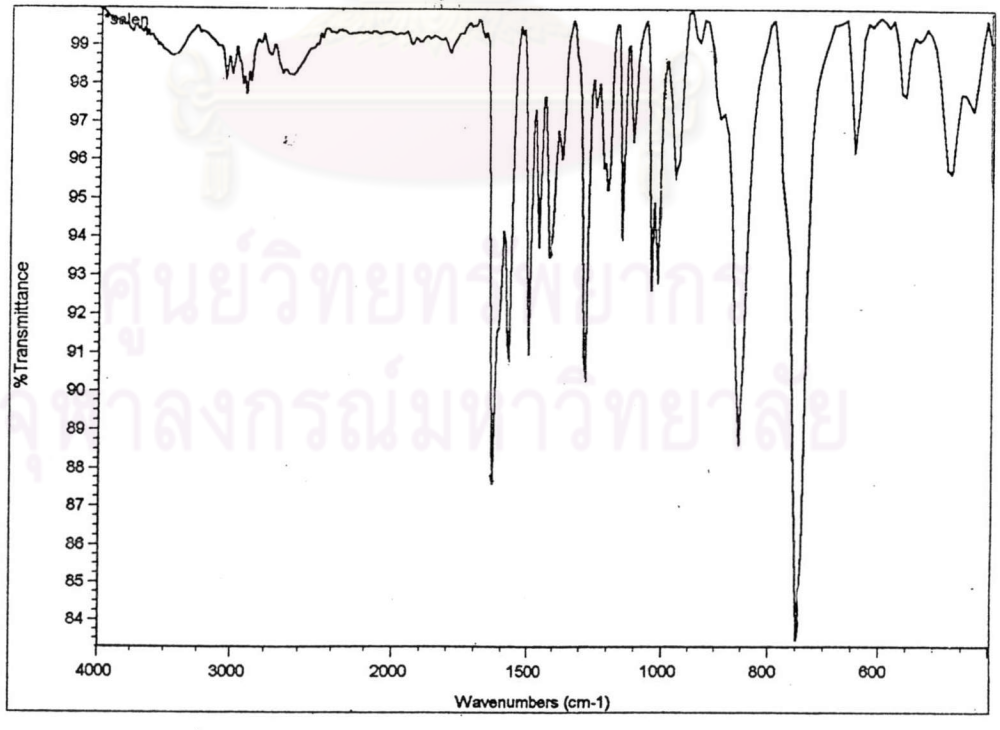

Figure 5.13 FT-IR spectrum of ligand (**c**).

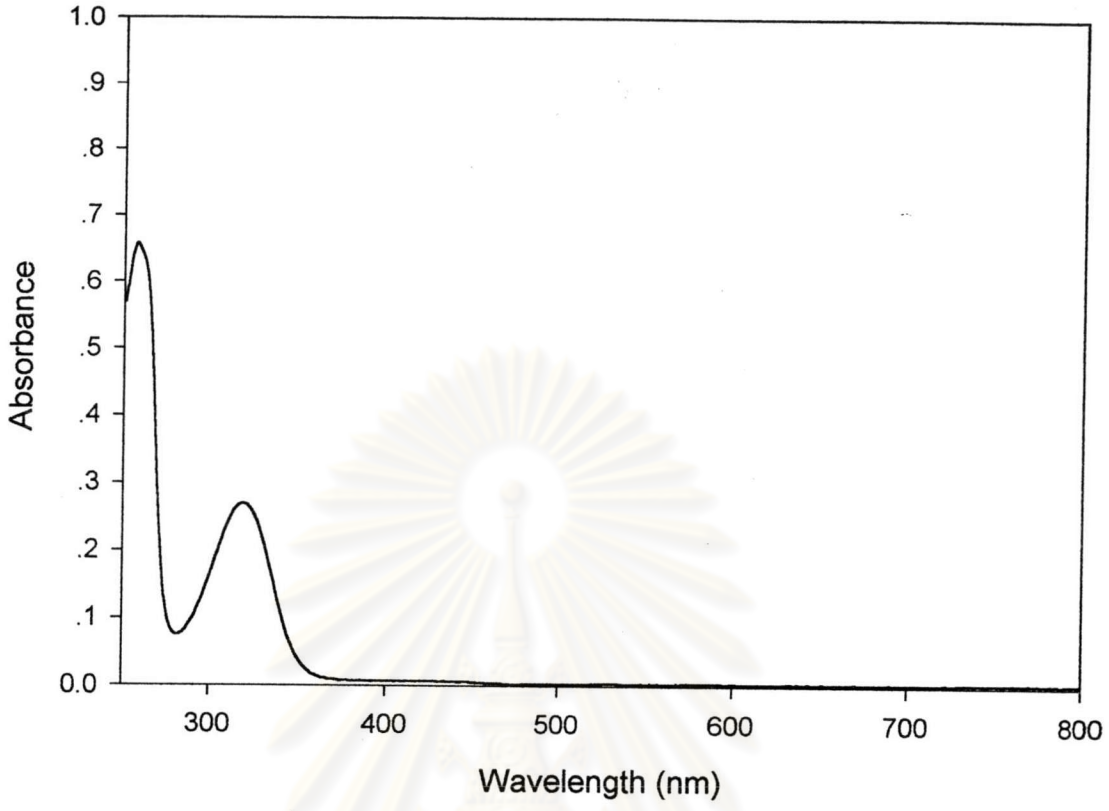

Figure 5.14 UV-visible spectrum of ligand (**c**).

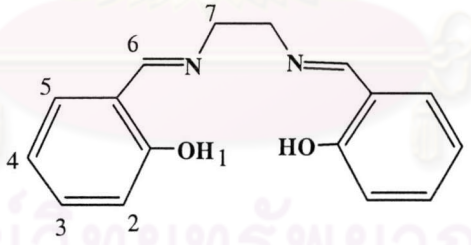

Table 5.8. ^{1}H-NMR data of ligand (**c**)

Chemical shift (ppm)	Multiplicity	Number of protons	Assignment
8.34	singlet	2H	H_6
7.29	doublets of triplet	2H	H_5 (J = 7.9, 1.8 Hz)
7.21	doublets of doublet	2H	H_3 (J = 7.8, 1.7 Hz)
6.92	doublet	2H	H_4 (J = 8.2 Hz)
6.83	doublets of triplet	2H	H_2 (J = 7.4, 1.1 Hz)
3.93	singlet	4H	H_7

The ^{1}H-NMR of ligand (c) showed a singlet peak at 8.34 ppm that is assigned to imine protons. Multiplet peaks at range 7.29-6.83 ppm are assigned to aromatic ring protons. A broad peak of hydroxy protons at 13.2 ppm cannot be seen in this ^{1}H-NMR spectrum.

Table 5.9. FT-IR data of ligand (**c**)

Wave number (cm^{-1})	Assignment
3430	O-H stretching
3054	C-H aromatic stretching
2900	C-H aliphatic stretching
1635	C=N stretching
1280	C-O stretching
1149	C-N stretching
1018	C-C stretching

FT-IR spectrum showed broad peak of O-H stretching at 3430 cm^{-1}, two weak peaks of C-H stretching at 3054 and 2900 cm^{-1}, strong sharp peak of C=N stretching at 1635 cm^{-1} and medium peak of C-O stretching at 1280 cm^{-1}. The UV- visible spectrum of ligand (**c**) showed λ_{max} at 258 and 318 nm of aromatic ring Π-bond and C=N.

5.1.6 Fe(III)salen complex, **cpx 3c**

The synthesis of **cpx 3c** was as follows:

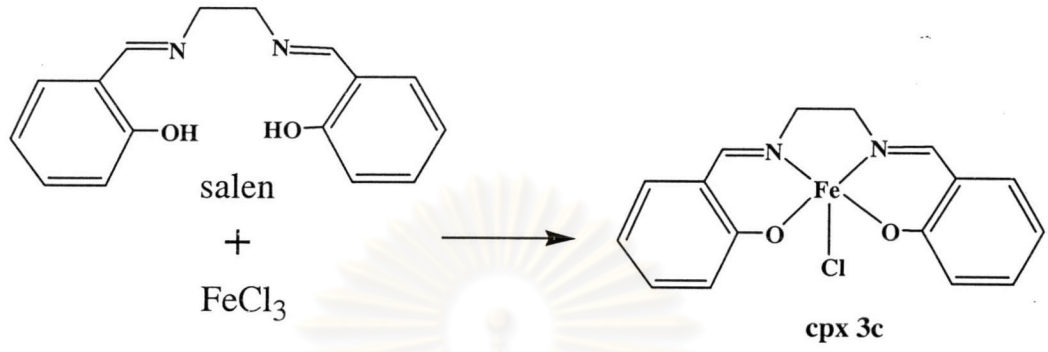

cpx 3c **(16)**

The Fe(III) salen complex as dark purple solids (43 %yield) was synthesized by directly treating one equivalent of $FeCl_3$ with the one equivalent of salen in ethanol. Molecular formula of **cpx 3c** calculated from elemental analysis was $C_{16}H_{14}N_2O_2FeCl$. FT-IR spectrum showed two peaks of C-H stretching at 3054 and 2900 cm^{-1}, a strong sharp peak of C=N stretching at 1627 cm^{-1}, a medium peak of C-O stretching at 1303 cm^{-1} and a weak peak of C-N stretching at 1126 cm^{-1}. The new absorption band of **cpx 3c** from UV-visible spectrum was at λ_{max} 475 nm.

It can be noticed from the comparison of FT-IR spectra of this iron complex (Figure 5.15 and Table 5.10) and salen that the band of O-H stretching (3430 cm^{-1}) was disappeared when the complex was formed.

The FT-IR spectrum, UV-visible spectrum and the FT-IR assignment of peak of this complex were shown in Figures 5.15-5.16 and Table 5.10 respectively.

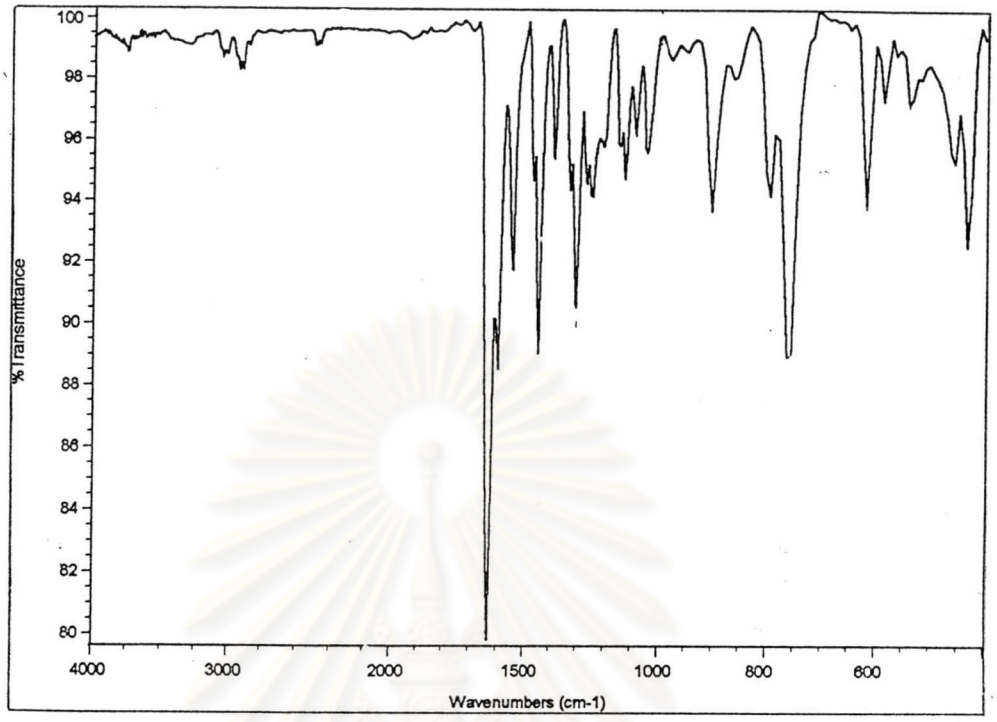

Figure 5.15 FT-IR spectrum of **cpx 3c**.

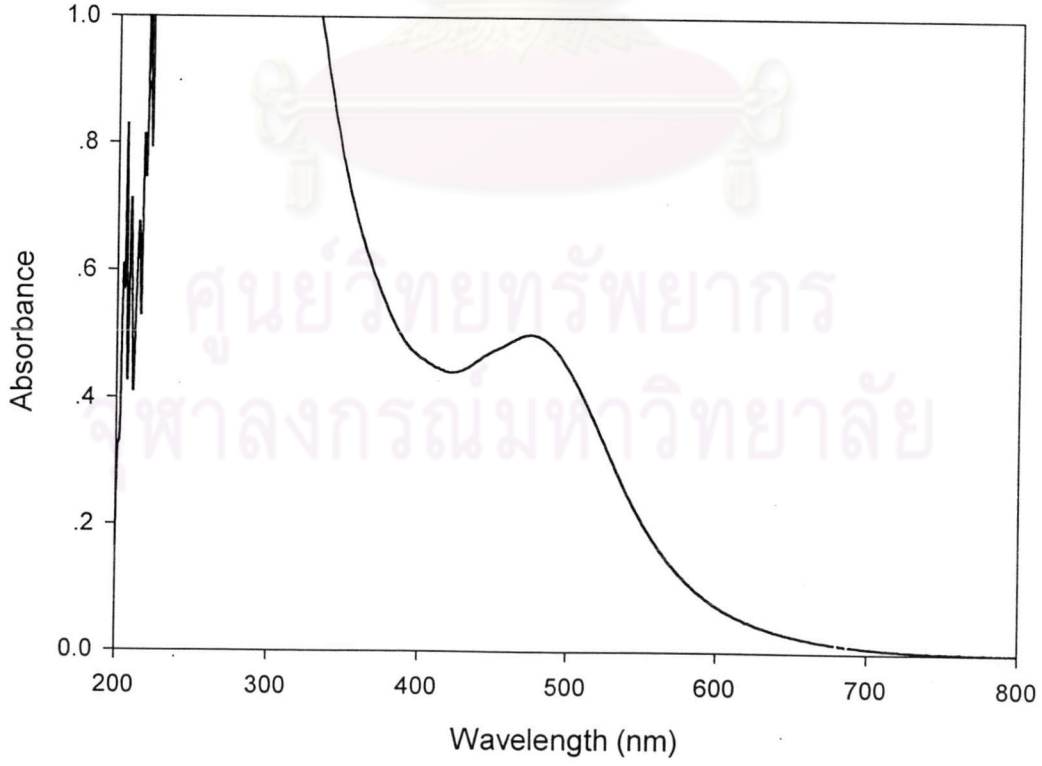

Figure 5.16 UV-visible spectrum of **cpx 3c**.

Table 5.10. FT-IR data of **cpx 3c**

Wave number (cm^{-1})	Assignment
3054	C-H aromatic stretching
2900	C-H aliphatic stretching
1627	C=N stretching
1303	C-O stretching
1126	C-N stretching
1041	C-C stretching

5.2 Polymerization of 1-hexene

5.2.1 Polymerization by MAO cocatalyst

5.2.1.1 Polymerization of 1-hexene with $[RHN(CH_2)_3NHR]FeCl_3$ (R = 2,6-^{i}Pr C_6H_3) (**cpx 1a**)/MAO

The effects of amount of catalyst, Al/Fe mole ratio and polymerization temperature were investigated by varying the catalyst concentration from $5.0x10^{-6}$ to $15.0x10^{-6}$ mol, Al/Fe mole ratio of 500, 1000, 2000 and 3000 and polymerization temperature at 0°C, 30°C and 50°C. The experimental results were shown in Table 5.11.

Table 5.11. Polymerization of 1-hexene catalyzed by **cpx 1a**/MAO using various polymerization conditions

Entry	Amount of catalyst (mol)	Al/Fe mole ratio	T_p (°C)	Product (mg)	%Yield	Activity (kg polymer mol cat^{-1})
1	$5.0x10^{-6}$	1000	30	14.2	0.4	2.8
2	$10.0x10^{-6}$	1000	30	138.7	4.1	13.9
3	$15.0x10^{-6}$	1000	30	104.5	3.1	6.9
4	$10.0x10^{-6}$	500	30	19.0	0.6	1.9
5	$10.0x10^{-6}$	2000	30	145.6	4.3	14.6
6	$10.0x10^{-6}$	3000	30	67.1	2.0	6.7
7	$10.0x10^{-6}$	1000	0	trace	-	-
8	$10.0x10^{-6}$	1000	50	224.8	6.7	22.5
9	$10.0x10^{-6}$	1000*	50	213.0	6.3	21.3

t_p 24 h and 1-hexene 5.00 mL (39.98 mmol, 3.36 g), * dried MAO = MAO (toluene solution) was evaporated in vacuo and was used as a white solid.

The results from entries 1-3 showed that the highest catalytic activity was obtained at $10x10^{-6}$ mol catalyst. Increasing the mole of catalyst caused the decreasing in the activity. This might be caused by the decreasing of active species due to the dimerization of catalyst forming inactive species. This result was concerned with the metallocene catalyst system that can dimerization when the catalyst concentration is increased. Additionally, the activity was decreased because the termination rate (that is β-H transfer to metal) increased when the excess amount of catalyst was used. It is well-known that β-H transfer to metal is a common chain-transfer process, especially for late-transition metal catalysts.[13]

A comparison between entries 2 and 4-6 showed that Al/Fe mole ratio at 1000 and 2000 gave similar and the highest activity. However, higher amount of MAO usually can stabilize the cation active species and also acts as an impurity scavenger. An increasing in Al/Fe mole ratio to 3000 in entry 6 resulted a decrease of activity because the termination step (chain transfer to aluminium) increased when the higher

amount of MAO was used.[13] This result was supported by an experiment of ethylene polymerization by $LFeCl_2$ catalyst (L = 2,6 - $(ArNCMe)_2C_5H_3N$). In a graphical illustration of MAO effect (Figure 5.17), it was seen that an increase in the MAO concentration enhanced the rate of chain transfer to aluminium which, combined with a constant rate of propagation and β-H transfer, wherein (a) is representative of a low MAO concentration and (b) is that of the higher MAO concentration.

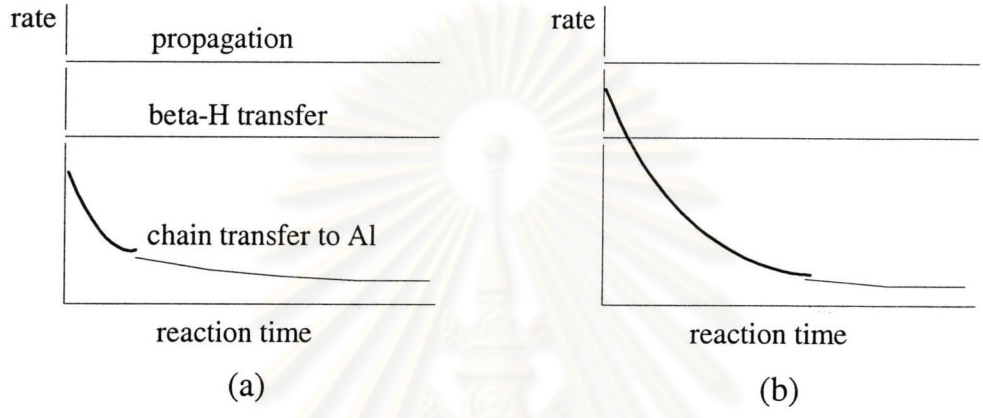

Figure 5.17 Schematic representations of the effects of different MAO concentration : (a) low MAO concentration, (b) high MAO concentration.

The influence of polymerization temperature that was investigated from entries 2, 7-8 showed that the temperature at 50°C gave the highest activity. An increasing in temperature results in higher propagation rate. These results can be explained by a widely accepted mechanism of propagation in which involves the initial formation of a ∏-complex of an olefin with the catalyst metal, followed by chain migratory insertion.

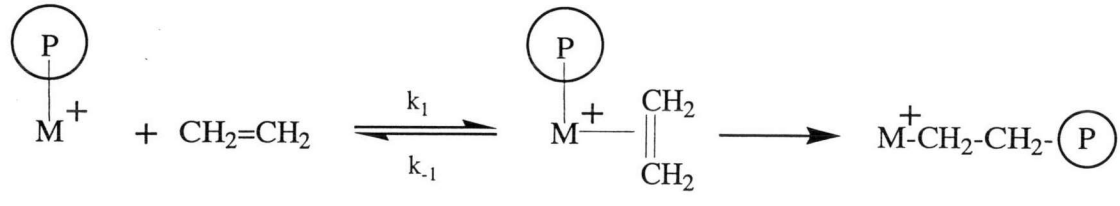

When ∏-olefin coordinated with metal center to form the ∏-olefin complex, this complex is more stable at the low temperature. Therefore, it is difficult for the complex to go on the propagation step by insertion process. This affects to the increase of activity with increasing polymerization temperature.

For entry 9, the same condition as entry 8 was used except that dried MAO was used. The result showed that the use of dried MAO which was prepared by removing toluene and an excess amount of $AlMe_3$ and used as a white solid, in place of ordinary MAO (toluene solution) did not affect in polymerization activity (the activity of both cases were the same). This contrasts to the case of ethylene polymerization by CpTi (O-2,6-$^{i}Pr_2C_6H_3)_2Cl$ which was found to be effective to increase polymer yield and activity when the dried MAO was used as a cocatalyst. Polymer yield (g)/activity (kg of PE/mol of Ti . h) for original MAO and dried MAO system were 1.4/77 and 3.2/441 respectively.[51]

5.2.1.2 Polymerization of 1-hexene with iron – based catalysts/MAO cocatalyst

The influence of different catalyst on 1-hexene polymerization was investigated. The results were shown in Table 5.12.

Table 5.12. Polymerization of 1-hexene catalyzed by various iron – based catalysts/MAO

Catalysts	Product (mg)	%Yield	Activity (kg polymer mol cat^{-1})
cpx 1a	138.7	4.1	13.9
cpx 2b	137.6	4.1	13.8
cpx 3c	trace	-	-

$10.0x10^{-6}$ mol catalyst, Al/Fe mole ratio of 1000, t_p 24 h, T_p 30°C and 1-hexene 5.00 mL (39.98 mmol, 3.36 g)

Iron complexes that can convert 1-hexene were **cpx 1a** and **cpx 2b**. Both give comparable %yield. The **cpx 3c** is inactive. The results showed that the activity of catalyst depends on ligand. Ligand in **cpx 1a** that is $RNH(CH_2)_3NHR$ (R = 2,6-$^{i}Pr_2C_6H_3$) had been used to react with $TiCl_4$ to synthesize catalyst for 1-hexene polymerization.[50] $RHN(CH_3)C=C(CH_3)C=NR$ (R = 2,6-$^{i}Pr_2C_6H_3$) which is ligand in **cpx 2b** also had been used to synthesize chromium catalyst for ethylene polymerization.[62] These mean that ligand (**a**) and (**b**) are appropriate for olefin polymerization.

5.2.2 Polymerization by boron cocatalyst

5.2.2.1 Polymerization of 1-hexene catalyzed by **cpx 1a**/$[Ph_3C]$ $[B(C_6F_5)_4]$ using various polymerization conditions

The influence of catalyst concentration, polymerization temperature (t_p) and Al/Fe mole ratio on 1-hexene polymerization was studied by varying catalyst concentration from $2.5x10^{-6}$ to $15.0x10^{-6}$ mol, temperature at -20°C, 0°C, 30°C and 50°C and Al/Fe mole ratio at 200 and 400 (mole of aluminium comes from the amount of used TIBA) using $[RHN(CH_2)_3NHR]FeCl_3$ (R = 2,6-$^{i}PrC_6H_3$) (**cpx 1a**) / $[Ph_3C]$ $[B(C_6F_5)_4]$. The experimental results were shown in Table 5.13.

Table 5.13. Polymerization of 1-hexene catalyzed by **cpx 1a**/$[Ph_3C][B(C_6F_5)_4]$ at different polymerization conditions

Entry	Amount of catalyst (mol)	Al/Fe mole ratio	T_p (°C)	Product (mg)	%Yield	Activity (kg polymer mol cat^{-1})
1	$2.5x10^{-6}$	200	0	17.3	0.5	6.9
2	$5.0x10^{-6}$	200	0	52.8	1.6	10.5
3	$10.0x10^{-6}$	200	0	128.2	3.8	12.8
4	$15.0x10^{-6}$	200	0	87.5	2.6	5.8
5	$10.0x10^{-6}$	200	-20	105.5	3.1	10.5
6	$10.0x10^{-6}$	200	30	83.9	2.5	8.4
7	$10.0x10^{-6}$	200	50	58.9	1.8	5.9
8	$10.0x10^{-6}$	400	0	144.2	4.3	14.4
9	$10.0x10^{-6}$	-	30	-	-	-
10	-	200	30	-	-	-

t_p 24 h, 1-hexene 5.00 mL (39.98 mmol, 3.36 g) and 1 equivalent of boron cocatalyst

From entries 1-4, the optimum amount of catalyst was $10x10^{-6}$ mol. The activity decreased with increasing mole of catalyst due to the dimerization of catalyst forming inactive species. Furthermore the termination rate (β-H transfer to metal) increased when higher amount of catalyst was used.[13]

From entries 3, 5-7, the optimum temperature was 0°C. The polymerization by boron cocatalyst system at low temperature gave higher activity than that at high temperature. Higher temperature led to reduced activity because of increasing rate of catalyst deactivation.[13]

Results from entries 3 and 8 showed that Al/Fe mole ratio of 400 gave higher activity than that of 200. Increasing amount of TIBA helped acting as an impurity scavenger.

From entries 9 and 10, respectively it also showed that no polymerization was occurred without catalyst or TIBA.

%Yield of products and activity obtained from **cpx 1a** and **cpx 2b** were very low. This could be due to the fact that the late transition complex catalysts generally exhibit reduced activities for olefin insertion and β-H elimination, which steadily competes with chain growth resulting in the formation of oligomer and low %yield. Additionally, the product that is colorless oil might be lost in the step of solvent evaporation. Souane and co-worker had studied the polymerization of 1-hexene by $LFeCl_2$ catalyst (L = 2,6-$(ArNCMe)_2C_5H_3N$) which was a very good catalyst for ethylene polymerization in 2002. They found that no polymer was obtained. They proposed that this might be due to an extremely slow propagation rate or to a poisoning of the catalytic sites by the monomer.[65] Additionally, oligomerization of 1-hexene by early and late transition metals has been reported. When 1-hexene was added to [t-BuNSN]$ZrMe_2$/$[Ph_3C][B(C_6F_5)_4]$ system, oligomerization of 1-hexene was observed. It was not clear whether this low degree of polymerization was due to inherently slow propagation or to a thermal instability of the cationic initiator and the intermediate cation that contains the growing polymer chain.[66] In addition, Zr(O-*n*-Pr)$_4$/$AlEt_2Cl$ system also produced oligomer of 1-hexene.[29]

5.2.2.2 Polymerization of 1-hexene catalyzed by **cpx 1a**/$[Ph_3C][B(C_6F_5)_4]$ with adding dichloromethane solvent

The effect of dichloromethane solvent in 1-hexene polymerization was investigated. The results were shown in Table 5.14.

Table 5.14. Polymerization of 1-hexene catalyzed by **cpx 1a**/$[Ph_3C][B(C_6F_5)_4]$ with adding dichloromethane solvent

Entry	Added solvent	Time (h)	Product (mg)	%Yield	Activity (kg polymer mol cat^{-1})
1	-	24	303.6	3.0	12.1
2	CH_2Cl_2	24	347.4	3.4	13.9

$10.0x10^{-6}$ mol catalyst, 1.5 equivalent of boron cocatalyst, T_p 30°C, Al/Fe 400 and 1-hexene 5.00 mL (39.98 mmol, 3.36 g)

The results from Table 5.14 showed that %yields of product between adding dichloromethane and without adding dichloromethane were the same. This means that the adding of dichloromethane did not affect in the increasing of %yield.

5.2.2.3 Comparison of boron cocatalysts

The effect of different cocatalyst on 1-hexene polymerization using [RHN$(CH_2)_3$NHR]$FeCl_3$ (R = 2,6-^{i}Pr C_6H_3) (**cpx 1a**) was investigated by varying types of cocatalyst; [$PhNMe_2H$][$B(C_6F_5)_4$] and [Ph_3C][$B(C_6F_5)_4$]. The experimental results were shown in Table 5.15.

Table 5.15. Polymerization of 1-hexene catalyzed by **cpx 1a** using different boron cocatalysts

Cocatalyst	Al/Fe mole ratio	Product (mg)	%Yield	Activity (kg polymer mol cat $^{-1}$)
[$PhNMe_2H$][$B(C_6F_5)_4$]	200	72.8	2.2	7.3
[Ph_3C][$B(C_6F_5)_4$]	200	83.9	2.5	8.4

$10.0x10^{-6}$ mol catalyst, 1 equivalent of boron cocatalyst, t_p 24 hr, T_p 30°C and 1-hexene 5.00 mL (39.98 mmol, 3.36 g)

[Ph_3C][$B(C_6F_5)_4$] gave the same activity as [$PhNMe_2H$][$B(C_6F_5)_4$].

5.2.2.4 Comparison of alkylating agent

The effect of different alkylating agent on 1-hexene polymerization using [RHN$(CH_2)_3$NHR]$FeCl_3$ (R = 2,6-^{i}Pr C_6H_3) (**cpx 1a**) was investigated by varying types of alkylating agent; TIBA (200 times of catalyst concentration), MeMgBr (3.5 times of catalyst concentration) and PhMgCl (3.5 times of catalyst concentration). The experimental results were shown in Table 5.16.

Table 5.16. Polymerization of 1-hexene catalyzed by **cpx 1a** using different alkylating agent

Alkylating agent	Product (mg)	%Yield	Activity (kg polymer mol cat $^{-1}$)
TIBA	72.8	2.2	7.3
MeMgBr	38.8	1.1	3.9
PhMgCl	58.8	1.8	5.9

10.0×10^{-6} mol catalyst, 1 equivalent of boron cocatalyst, t_p 24 hr, T_p 30°C and 1-hexene 5.00 mL (39.98 mmol, 3.36 g)

Using TIBA as alkylating agent gave better activity than using MeMgBr and PhMgCl as alkylating agent. It was believed that TIBA not only functions as an alkylating agent but also an impurity scavenger.

5.2.2.5 Polymerization of 1-hexene with various iron-base catalysts/$[Ph_3C][B(C_6F_5)_4]$ cocatalyst

The influence of different catalysts on 1-hexene polymerization was investigated. The results were shown in Table 5.17.

Table 5.17. Polymerization of 1-hexene catalyzed by various iron-based catalysts/$[Ph_3C][B(C_6F_5)_4]$

Catalysts	Product (mg)	%Yield	Activity (kg polymer mol cat^{-1})
cpx 1a	83.9	2.5	8.4
cpx 2b	38.3	1.1	3.8

10.0×10^{-6} mol catalyst, Al/Fe mole ratio of 200, t_p 24 hr, T_p 30°C and 1-hexene 5.00 mL(39.98 mmol, 3.36 g)

Cpx 1a gave higher activity than **cpx 2b**. The reason for the difference in the activity between **cpx 1a** and **cpx 2b** was not clear at this moment.

5.2.2.6 Polymerization of 1-hexene with *rac*-Et(Ind)$_2$ZrCl$_2$ catalyst / [PhNMe$_2$H] [B(C$_6$F$_5$)$_4$] cocatalyst

For comparison, 1-hexene polymerization with *rac*-Et(Ind)$_2$ZrCl$_2$ catalyst and [PhNMe$_2$H] [B(C$_6$F$_5$)$_4$] as cocatalyst was performed. Al/Zr mole ratio of 200 and 300 and polymerization time at 24 and 48 h was investigated. The experimental results were shown in Table 5.18.

Table 5.18. Polymerization of 1-hexene catalyzed by *rac*-Et(Ind)$_2$ZrCl$_2$ / [PhNMe$_2$H] [B(C$_6$F$_5$)$_4$] cocatalyst

Entry	Al/Zr (mole ratio)	t_p (h)	Product (g)	%Yield	Activity (kg polymer mol cat^{-1})
1	200	24	0.8100	24.1	162
2	300	48	2.5500	75.9	510

5.0x10^{-6} mol catalyst, 1 equivalent of [PhNMe$_2$H][B(C$_6$F$_5$)$_4$], T_p 30°C and 1-hexene 5.00 ml (39.88 mmol, 3.36 g)

The results from Table 5.18 showed that the increasing in Al/Zr mole ratio and polymerization time caused the increasing in yield and activity. For comparison with non-metallocene catalyst, this zirconocene catalyst gave higher %yield and activity than **cpx 1a** catalyst.

5.3 Characterization of polymer

5.3.2 Chemical structure determination

5.3.1.1 Carbon-13 nuclear magnetic resonance spectroscopy (^{13}C-NMR)

Carbon-13 nuclear magnetic resonance (^{13}C NMR) spectroscopy is a tool for molecular structure analysis. The chemical shifts of poly(1-hexene) is in a range 45- 10 ppm. The assignments of the chemical shifts are shown in Tables 5.19-5.21. The ^{13}C-NMR spectra of products obtained with **cpx 1a**, **cpx 2b** and *rac*-Et(Ind)$_2$ZrCl$_2$ are shown in Figures 5.18-5.21.

Table 5.19. ^{13}C-NMR data of product obtained with [RHN$(CH_2)_3$NHR]$FeCl_3$ (**cpx 1a**) catalyst (reference is atactic polyhexene)

Chemical shift (Exp.) (ppm)	Chemical shift (ref.[50]) (ppm)	Assignment
42	41	C_a
35	34	C_b
32	33	C_c
29	29	C_d
23	24	C_e
14	14	C_f

Table 5.20. ^{13}C-NMR data of product obtained with [RHN(CH_3)C=C(CH_3) C=NR] $FeCl_3$ (**cpx 2b**) catalyst (reference is atactic polyhexene)

Chemical shift (Exp.) (ppm)	Chemical shift (ref.[50]) (ppm)	Assignment
40	41	C_a
35	34	C_b
32	33	C_c
29	29	C_d
23	24	C_e
14	14	C_f

Table 5.21. ^{13}C-NMR data of poly(1-hexene) obtained with *rac*-Et(Ind)$_2$ZrCl$_2$ catalyst (reference is isotactic poly(1-hexene))

Chemical shift (Exp.) (ppm)	Chemical shift (ref.[55]) (ppm)	Assignment
40	40	C_a
35	35	C_c
32	32	C_b
29	29	C_d
23	23	C_e
14	14	C_f

Products that obtained with iron-based catalysts; **cpx 1a** and **cpx 2b** are atactic polymer. This was identified by the comparison of ^{13}C-NMR spectra of the products and reference atactic poly(1-hexene) in Figures 5.22-5.24. Steric bulkiness of the auxiliary ligand in metal complex plays an important role for the microstructure of the polymer product. Ligand in **cpx 1a** that is RNH(CH$_2$)$_3$NHR (R = 2,6-iPr$_2$C$_6$H$_3$) had been studied by forming complex with TiCl$_4$; [RN(CH$_2$)$_3$NR]TiCl$_2$. This titanium catalyst that activated with MAO and [Ph$_3$C][B(C$_6$F$_5$)$_4$] cocatalyst generated atactic poly(1-hexene).[50]

Poly(1-hexene) as white rubber-like solid obtained by *rac*-Et(Ind)$_2$ZrCl$_2$ catalyst was isotactic poly(1-hexene). This result was confirmed by ^{13}C-NMR spectrum compared with the reference. This zirconium catalyst is a well-known catalyst for producing isotactic poly(1-hexene).[48]

A comparison between ^{13}C-NMR spectra of atactic and isotactic poly(1-hexene) reveals that atactic poly(1-hexene) showed broad and multiplet peak while isotactic poly(1-hexene) showed sharp singlet peak.

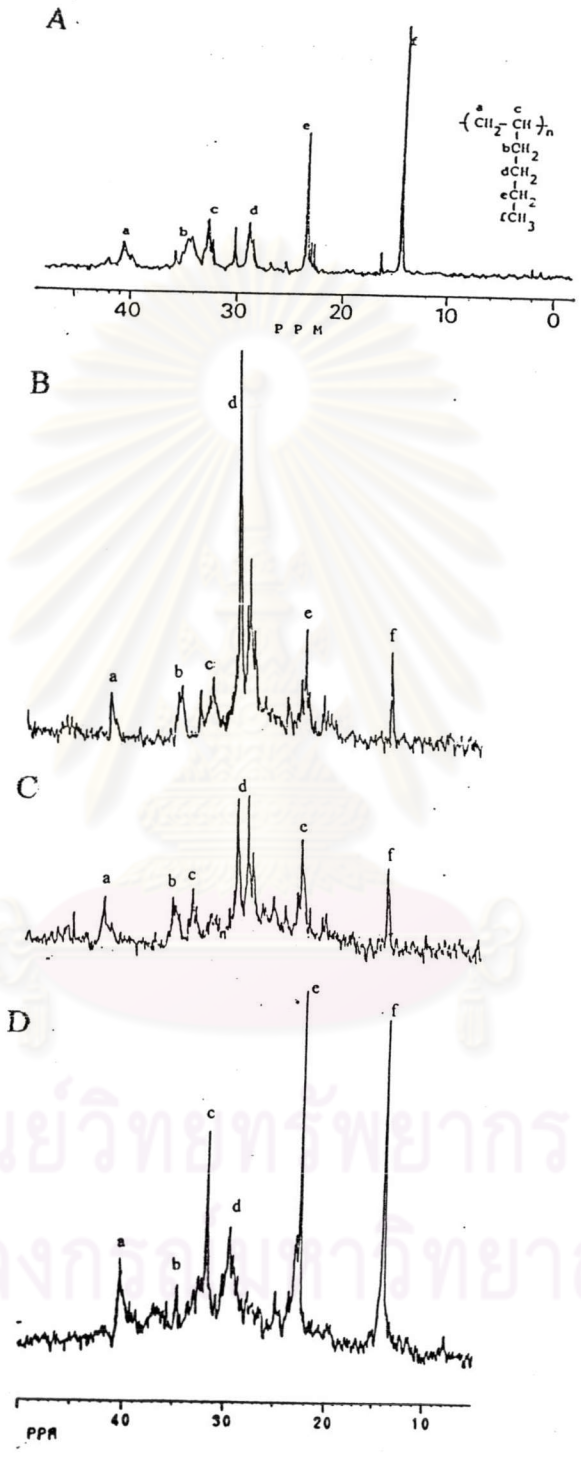

Figure 5.18 ^{13}C-NMR spectra of product obtained with $[RHN(CH_2)_3NHR]FeCl_3$ (**cpx 1a**)/MAO.

A) reference atactic poly(1-hexene)[50] B) $10x10^{-6}$mol catalyst, Al/Fe 2000,30°C C) $10x10^{-6}$mol catalyst, Al/Fe 1000, 30°C D) $10x10^{-6}$mol catalyst, Al/Fe 1000, 50°C

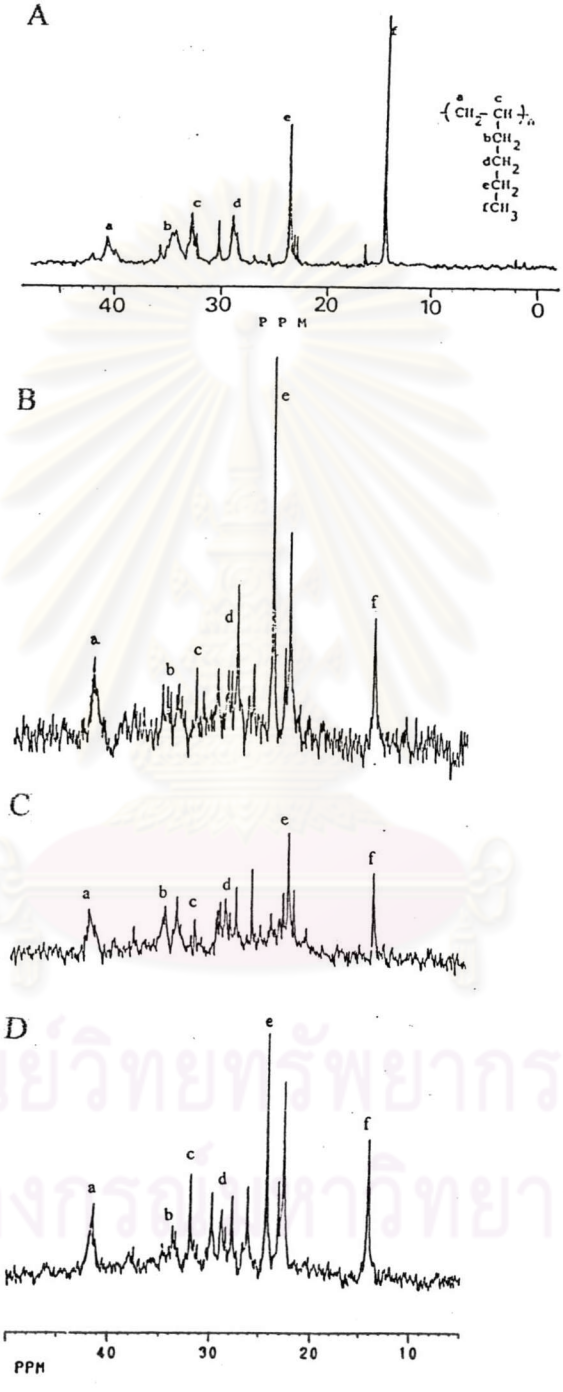

Figure 5.19 ^{13}C-NMR spectra of product obtained with $[RHN(CH_2)_3NHR]FeCl_3$ (**cpx 1a**)/$[Ph_3C][B(C_6F_5)_4]$.

A) reference atactic poly(1-hexene)[50] B) $10x10^{-6}$mol catalyst, TIBA 400, 0°C

C) $10x10^{-6}$mol catalyst, TIBA 200, 30°C D) $10x10^{-6}$mol catalyst, TIBA 200, 50°C

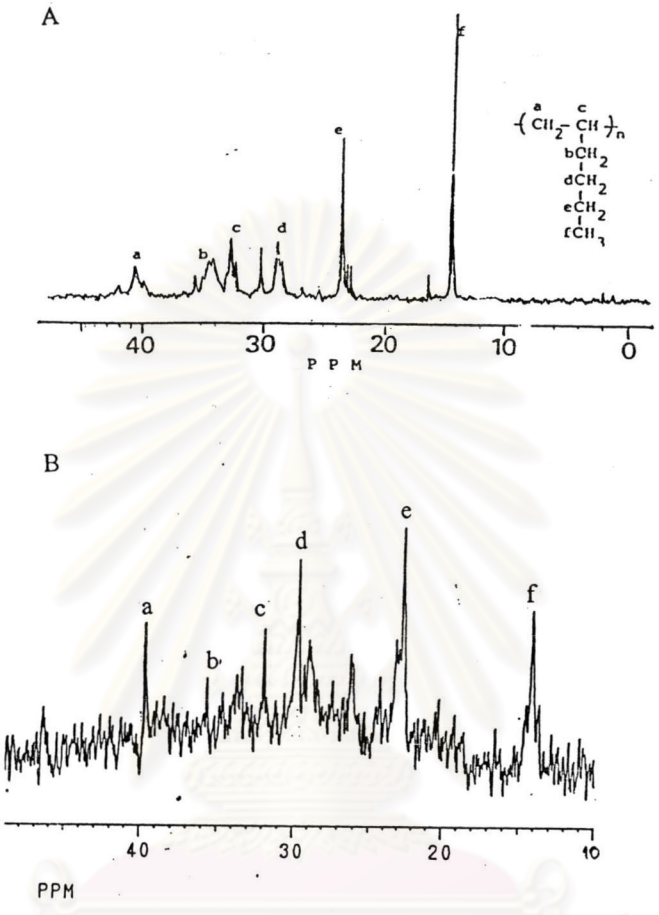

Figure 5.20 ^{13}C-NMR spectra of product obtained with [RHN(CH_3)C=C(CH_3) C=NR]$FeCl_3$ (**cpx 2b**).

A) reference atactic poly(1-hexene)[50]

B) **cpx 2b**/[Ph_3C][$B(C_6F_5)_4$] cocatalyst

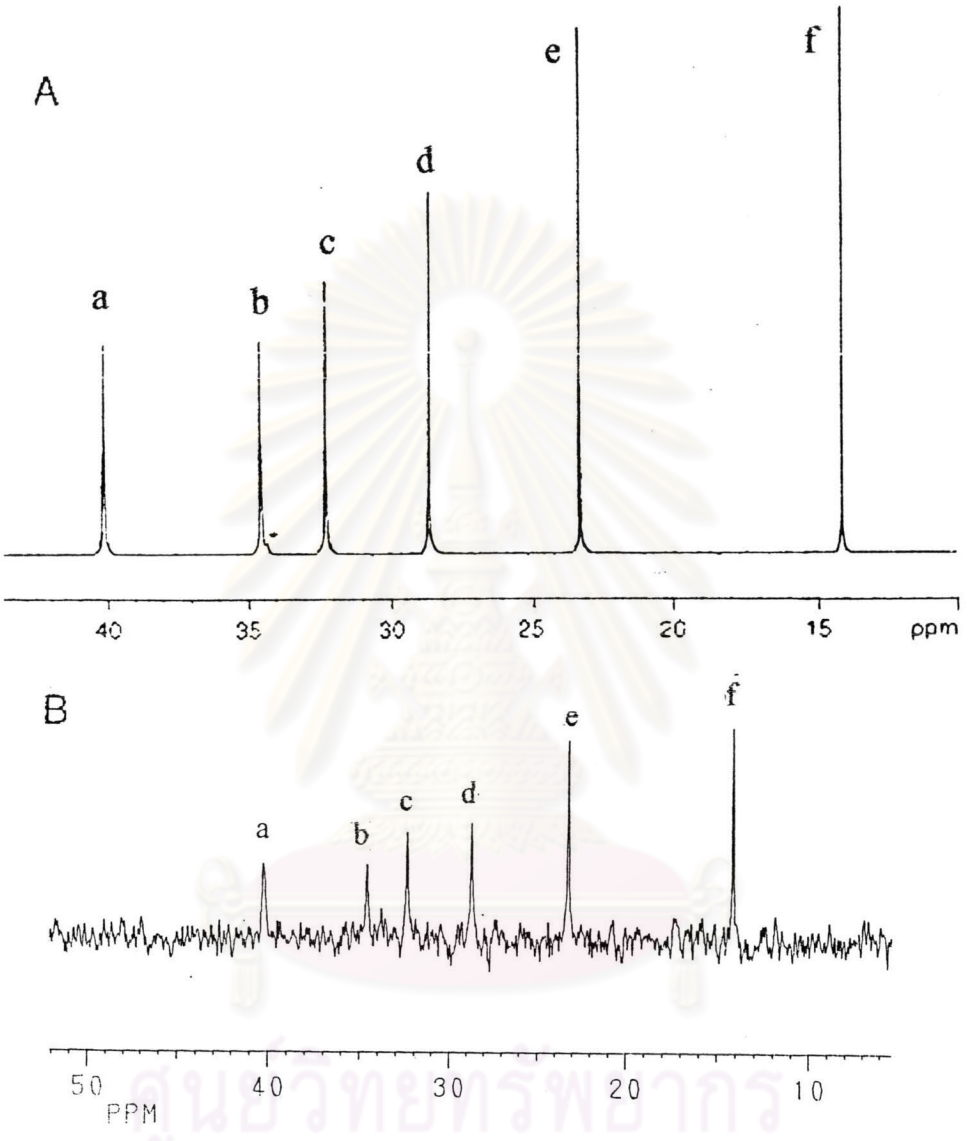

Figure 5.21 ^{13}C-NMR spectra of poly(1-hexene) obtained with *rac*-Et(Ind)$_2$ZrCl$_2$.
A) reference isotactic poly(1-hexene)[55]
B) *rac*-Et(Ind)$_2$ZrCl$_2$ /[PhNMe$_2$H][B(C$_6$F$_5$)$_4$] cocatalyst

5.3.1.2 Proton nuclear magnetic resonance spectroscopy (^{1}H-NMR)

The ^{1}H-NMR spectroscopy is a helpful technique to identify the end group of polymer. There is a report about end-group analysis of the oligohexenes formed (^{1}H-NMR) showed the chemical shift of internal double bonds (δ = 5.37-5.34), vinylidene end group ($H_2C=C(R)R'$, δ = 4.72-4.56) and vinyl end group {$H_2C=CHCH_2R$, δ = 5.80 (m, 1H, $H_2C=CHCH_2R$) and δ = 5.01-4.90 (m, 2H, $H_2C=CHCH_2R$)}.[41] The ^{1}H-NMR signal of poly(1-hexene) end group consists of vinylidene end group at 4.8-4.6 ppm, internal double bond at 5.4-5.2 ppm, vinyl end group at 5.2-5.0 ppm and saturated end group at 1.3 ppm ($-CH_2-$) and at 0.8 ppm ($-CH_3$). The ^{1}H-NMR spectrum of product obtained from *rac*-Et(Ind)$_2$ZrCl$_2$ and **cpx 1a** were shown in Figures 5.22-5.23.

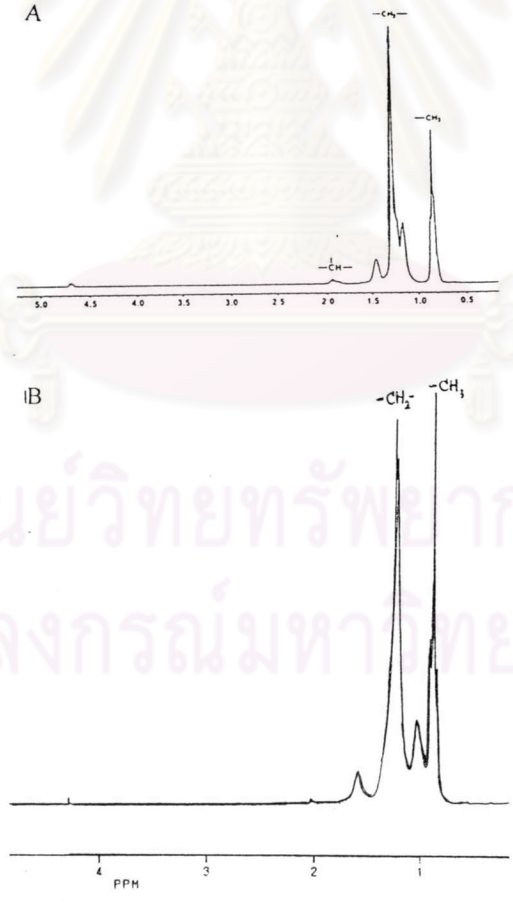

Figure 5.22 ^{1}H-NMR spectra of poly(1-hexene).
A) reference isotactic poly(1-hexene)[55] B) *rac*-Et(Ind)$_2$ZrCl$_2$/[PhMe$_2$NH][B(C$_6$F$_5$)$_4$]

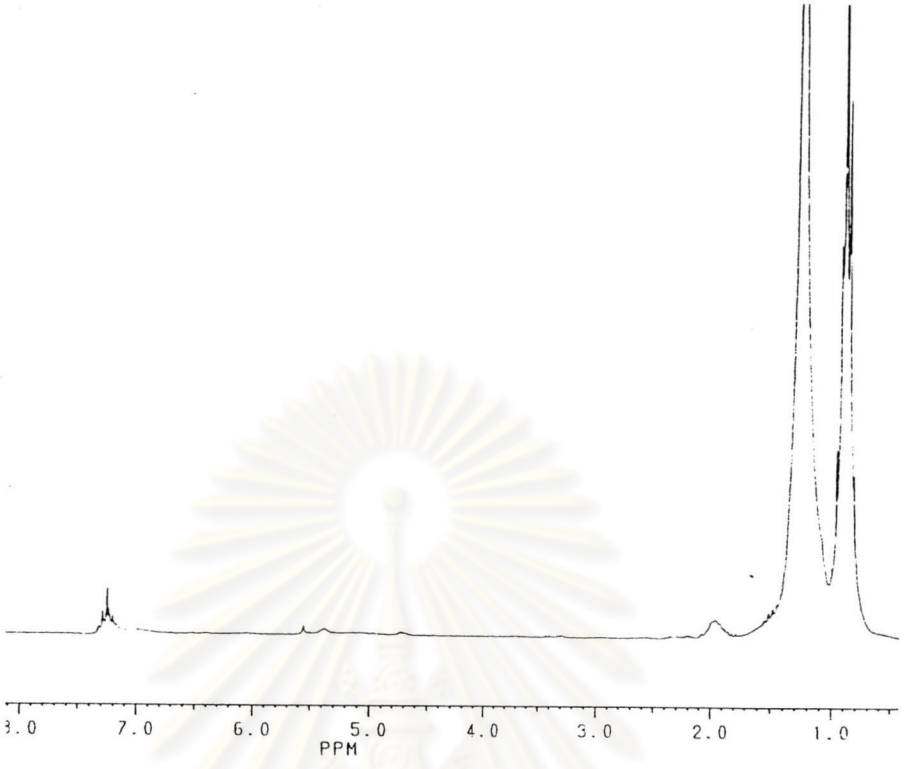

Figure 5.23 ^{1}H-NMR spectrum of product from **cpx 1a**/$[Ph_3C][B(C_6F_5)_4]$. ($10x10^{-6}$ mol catalyst, Al/Fe 400 T_p 30°C and t_p 24 h)

^{1}H-NMR spectrum of poly(1-hexene) in Figure 5.22 indicated that there are two different types of end group. The vinylidene signal is at 4.6 ppm and the saturated end group signal is at 0.8 ppm. These mean that there are two types of termination process; β-H transfer, giving vinylidene end group and chain transfer to aluminum, giving saturated end group. Figure 5.23 showed that ^{1}H-NMR spectrum of product from **cpx 1a** consisted of the vinylidene end group signal at 5.65 and 4.72 ppm, the internal double bond signal at 5.35 ppm. These chemical shifts concern with a report about end-group analysis of the oligohexenes formed (^{1}H-NMR) showed the chemical shift of internal double bonds (δ = 5.37-5.34), vinylidene end group {H_2C=$CHCH_2R$, δ = 5.01-4.90 (m, 1H, H_2C=C*H*CH_2R) and δ = 4.72-4.56δ (m, 2H, *H_2*C=$CHCH_2R$)}. [41] These indicated that there are three types of product's end group; β-H transfer, giving vinylidene end group, rearrangement, giving internal double bond and chain transfer to aluminum, giving saturated end group.

5.3.1.3 Gas chromatography-mass spectrometry (GC-MS) and gas chromatography (GC)

Gas chromatography-mass spectrometry (GC-MS) and gas chromatography (GC) are methods used for identifiying products. Gas chromatogram of polymerization products obtained by using **cpx 1a**/$[Ph_3C][B(C_6F_5)_4]$ system ($10.0x10^{-6}$ mol catalyst, 1 equivalent of boron cocatalyst, Al/Fe mole ratio 200, t_p 24 h and T_p 50°C) and using **cpx 2b** /$[Ph_3C][B(C_6F_5)_4]$ system ($10.0x10^{-6}$ mol catalyst, 1 equivalent of boron cocatalyst, Al/Fe mole ratio 200, t_p 24 h and T_p 30°C) were shown in Figures 5.24-5.25. Their mass spectra of each chromatogram were shown in Figures 5.26-5.32.

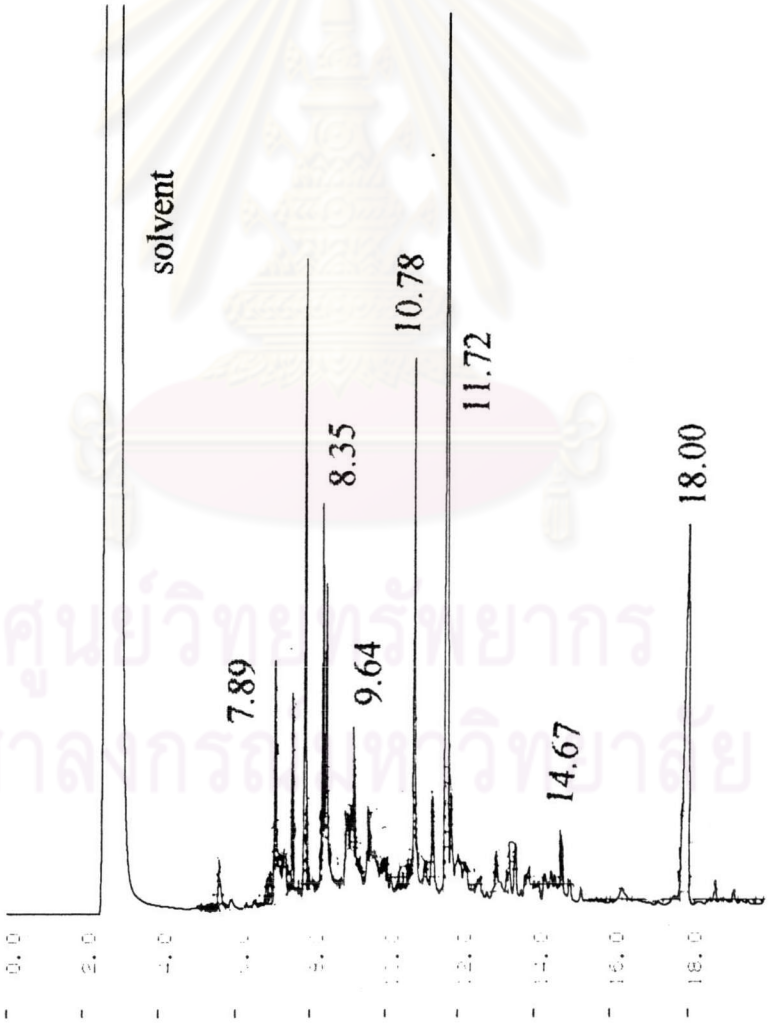

Figure 5.24 Gas chromatogram of polymerization product obtained by **cpx 1a/** $[Ph_3C][B(C_6F_5)_4]$ system ($10.0x10^{-6}$ mol catalyst, 1 equivalent of boron cocatalyst, Al/Fe mole ratio 200, t_p 24 h and T_p 50°C).

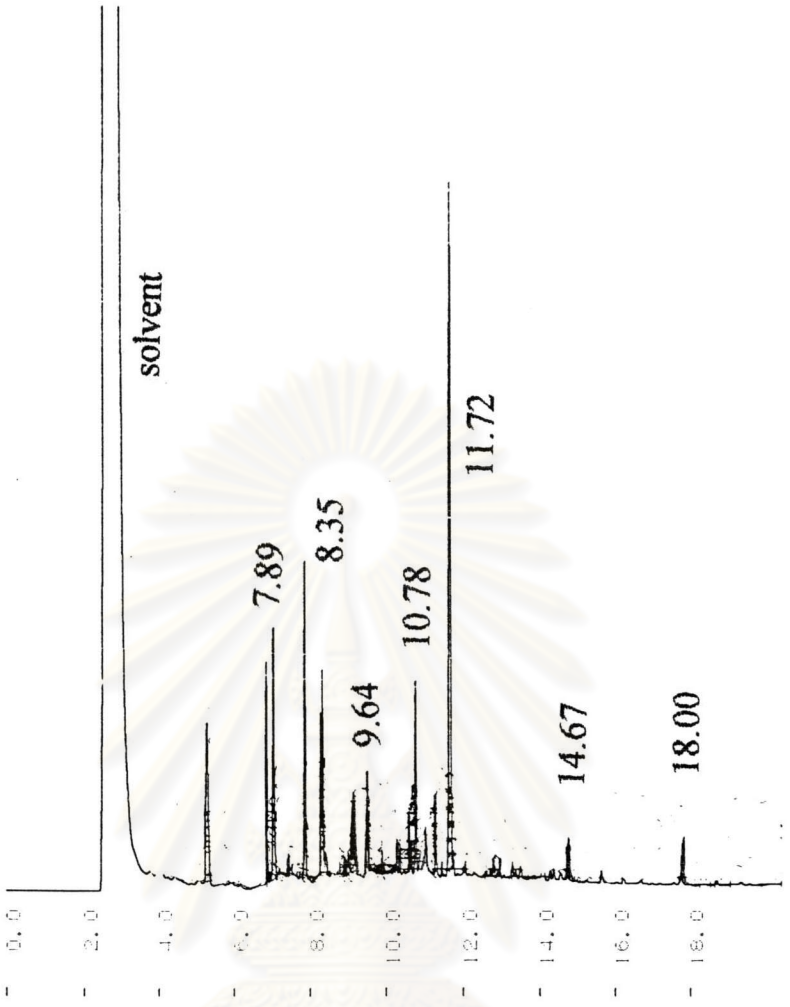

Figure 5.25 Gas chromatogram of polymerization product obtained by **cpx 2b/** $[Ph_3C][B(C_6F_5)_4]$ system ($10.0x10^{-6}$ mol catalyst, 1 equivalent of boron cocatalyst, Al/Fe mole ratio 200, t_p 24 h and T_p 30°C).

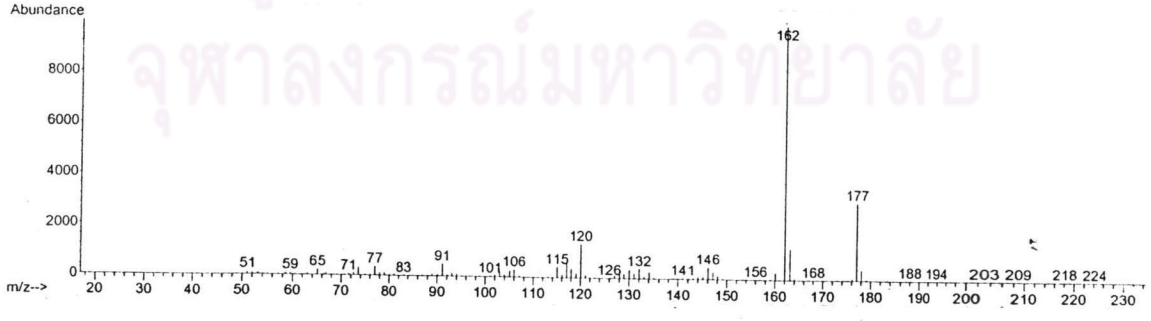

Figure 5.26 Mass spectrum of gas chromatographic peak at retention time of 7.89.

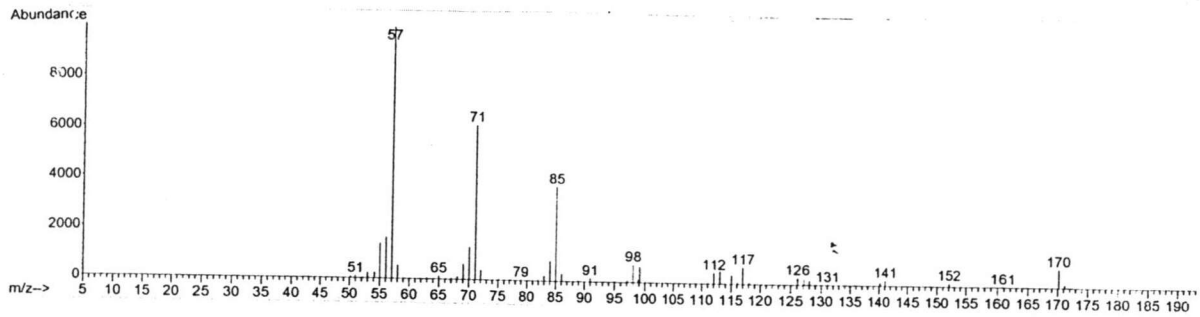

Figure 5.27 Mass spectrum of gas chromatographic peak at retention time of 8.35.

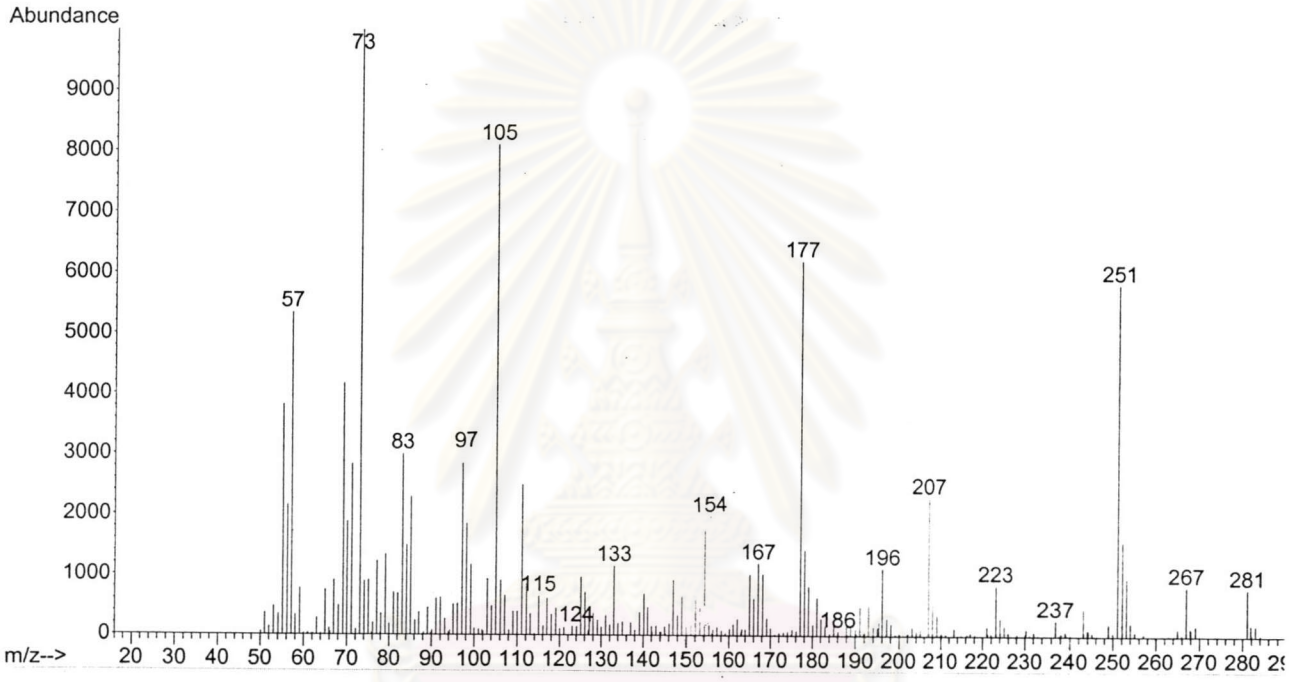

Figure 5.28 Mass spectrum of gas chromatographic peak at retention time of 9.64.

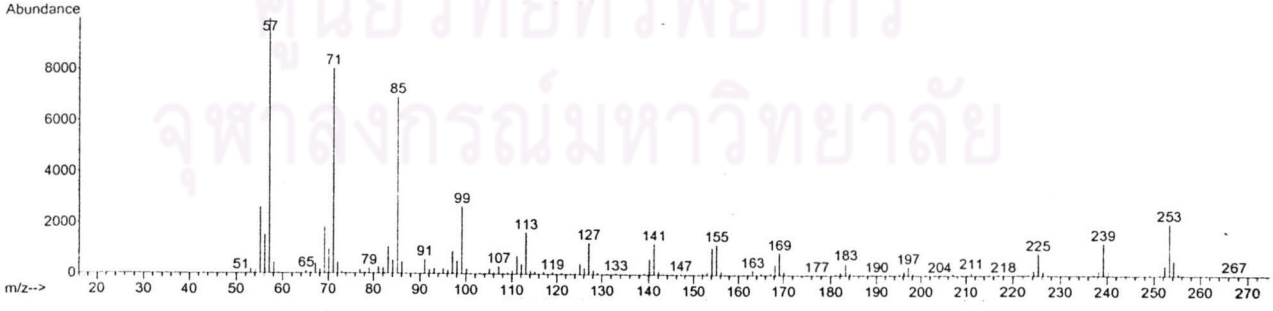

Figure 5.29 Mass spectrum of gas chromatographic peak at retention time of 10.78.

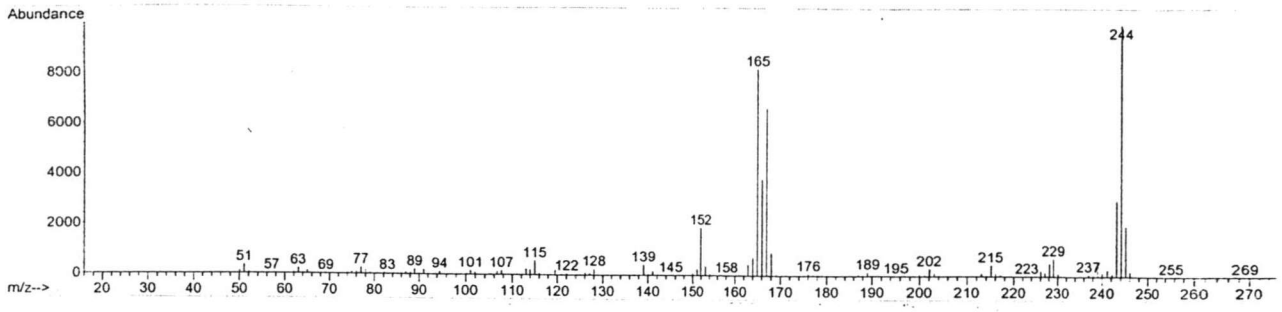

Figure 5.30 Mass spectrum of gas chromatographic peak at retention time of 11.72.

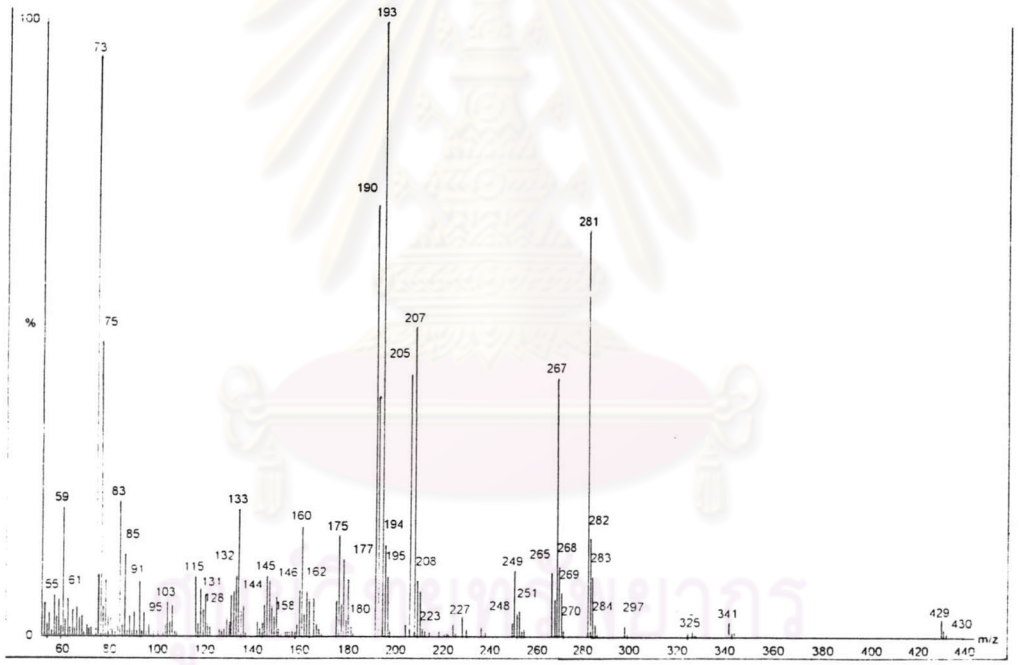

Figure 5.31 Mass spectrum of gas chromatographic peak at retention time of 14.67.

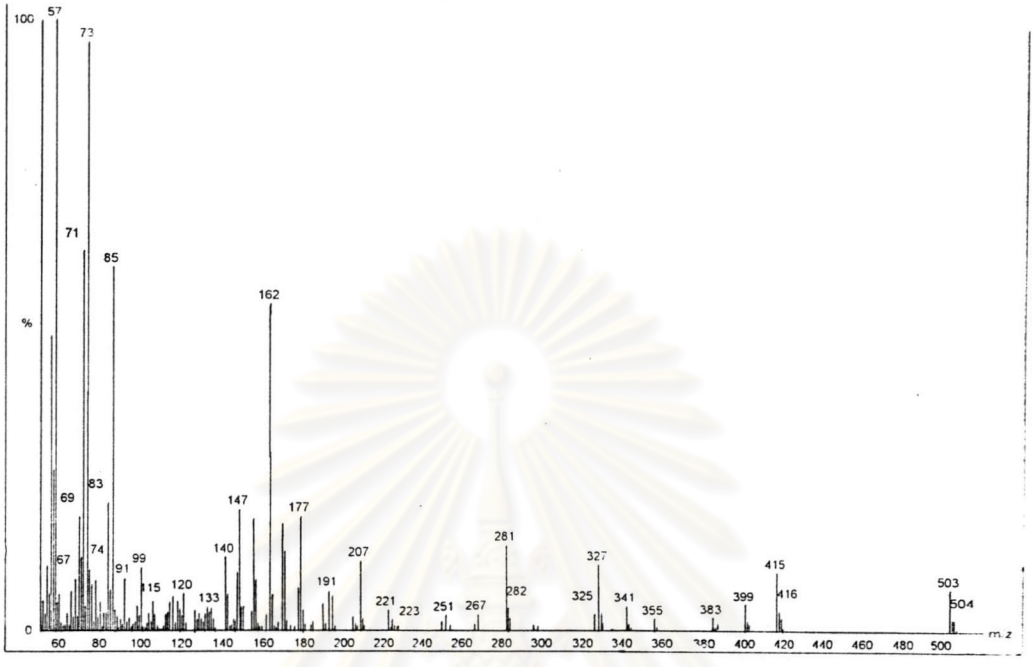

Figure 5.32 Mass spectrum of gas chromatographic peak at retention time of 18.00.

The results from GC-MS in Figures 5.24-5.32 revealed that gas chromatographic peak at time 7.89, 8.35, 9.64, 10.78, 11.72, 14.67 and 18.00 were ligand of **cpx 1a** catalyst, dimer (saturated end group), trimer (vinylidene end group), trimer (saturated end group), Ph_3CH that came from $[Ph_3C][B(C_6F_5)_4]$ cocatalyst, pentamer (vinylidene end group) and hexamer (vinylidene end group) respectively. This result showed that the working up procedure should be improved because the product from polymerization was contaminated with catalyst and cocatalyst.

The fragmentation patterns of each mass spectrum in Figures 5.26-5.32 were shown in Schemes 5.2-5.7 respectively.

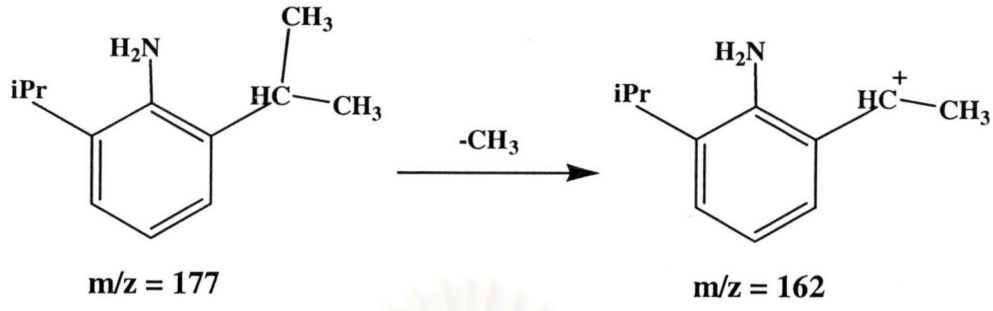

Scheme 5.2 The fragmentation pattern of 2,6-diisopropylaniline from Figure 5.26.

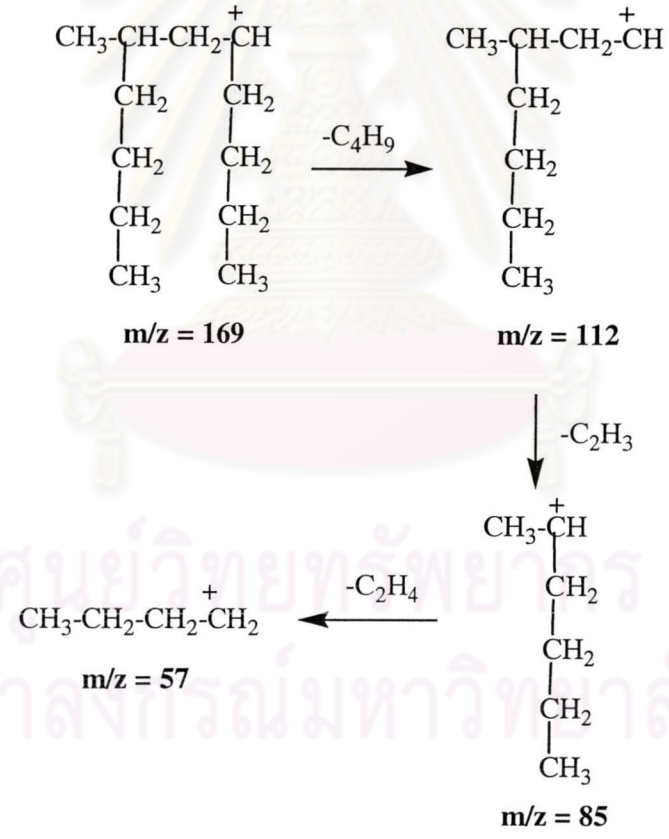

Scheme 5.3 The fragmentation pattern of dimer (saturated end group) from Figure 5.27.

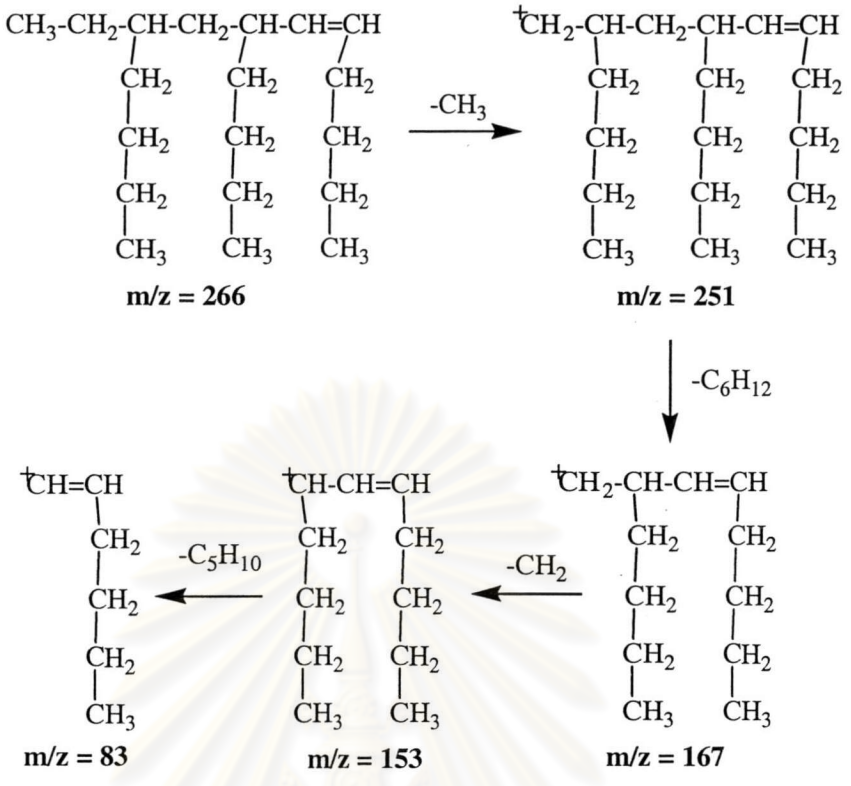

Scheme 5.4 The fragmentation pattern of trimer (vinylidene end group) from Figure 5.28.

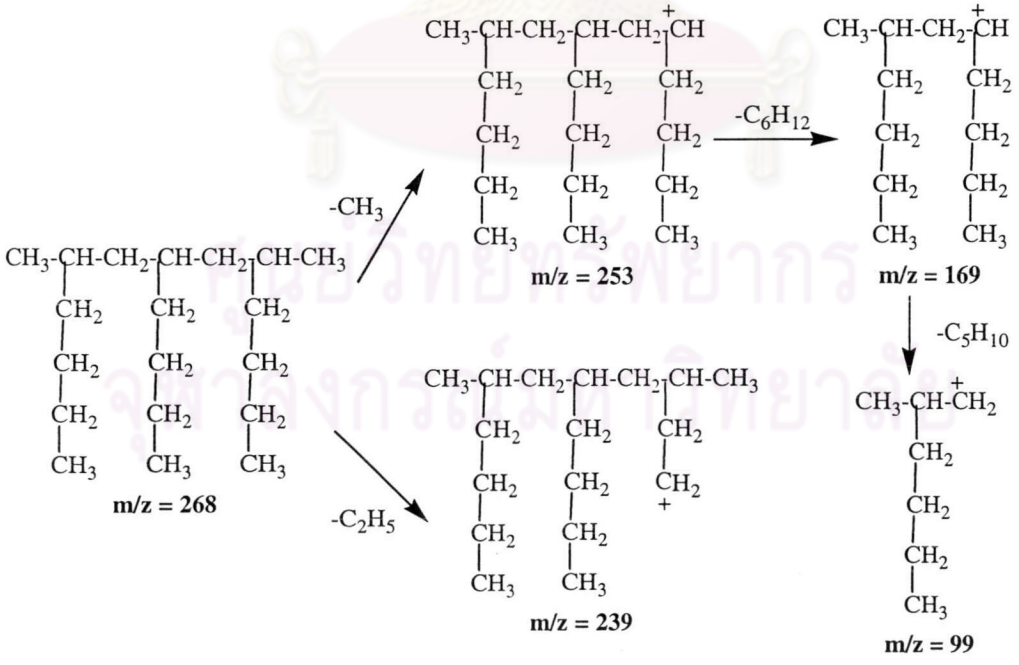

Scheme 5.5 The fragmentation pattern of trimer (saturated end group) from Figure 5.29.

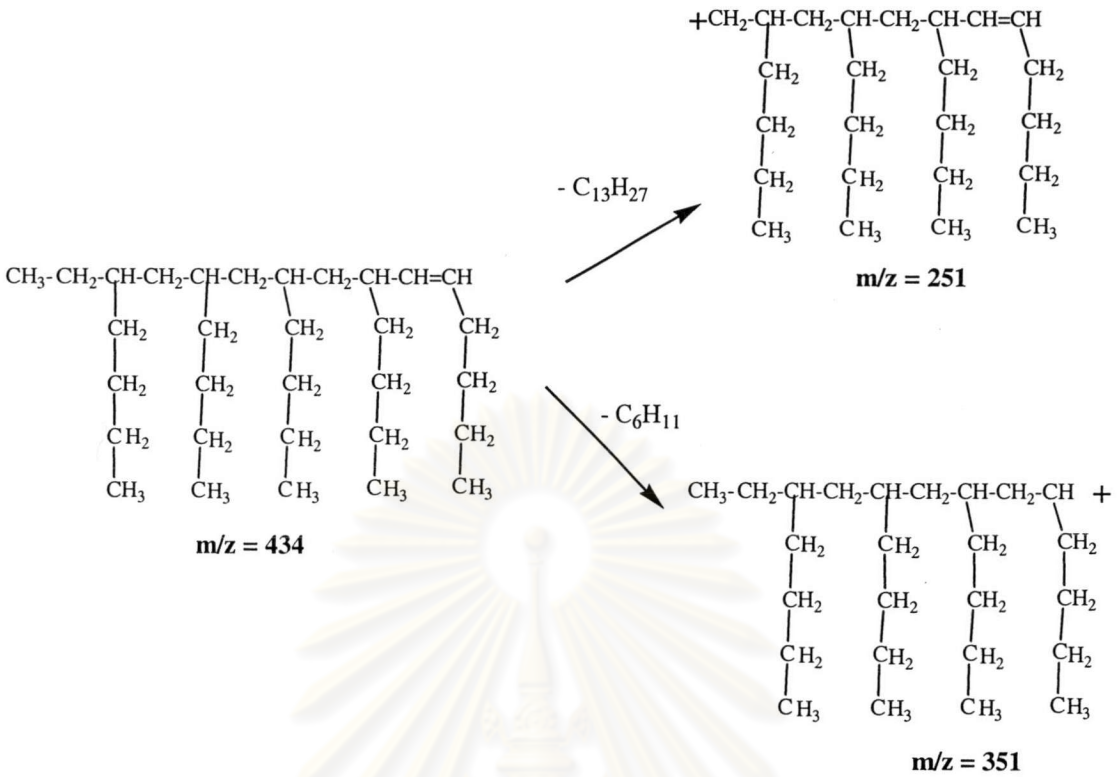

Scheme 5.6 The fragmentation pattern of pentamer (vinylidene end group) from Figure 5.31.

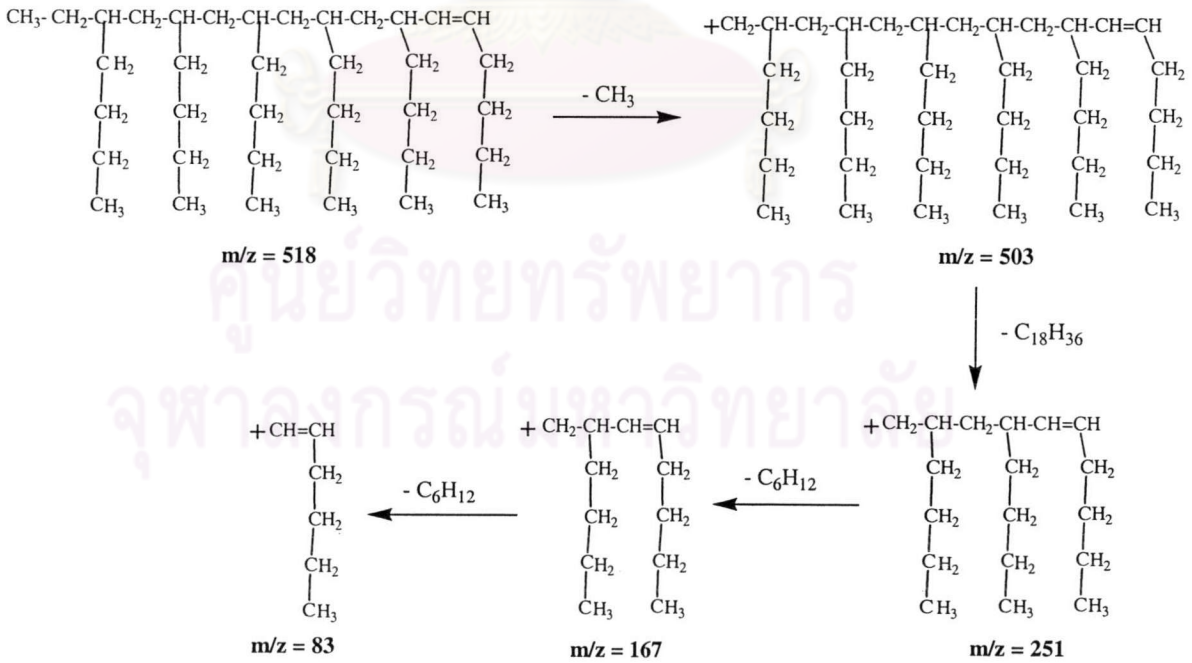

Scheme 5.7 The fragmentation pattern of hexamer (vinylidene end group) from Figure 5.32.

Gas chromatogram of obtained product by **cpx 2b**/[Ph_3C] [$B(C_6F_5)_4$] cocatalyst in Figure C from appendix section showed that a number of the products were the same as that from **cpx 1a**/[Ph_3C][$B(C_6F_5)_4$].

5.3.1.4 Infrared spectroscopy (IR)

The infrared spectroscopy is an effective method to determine the microstructure of polymer. It is sufficient to characterize the functional groups of poly (1-hexene) in the wave number of 400-4000 cm^{-1}. The FT-IR spectra of products obtained from **cpx 1a**, **cpx 2b** and *rac*-Et$(Ind)_2ZrCl_2$ were shown in Figures 5.33-5.36. The identification of the spectrum was summarized in Tables 5.22-5.24.

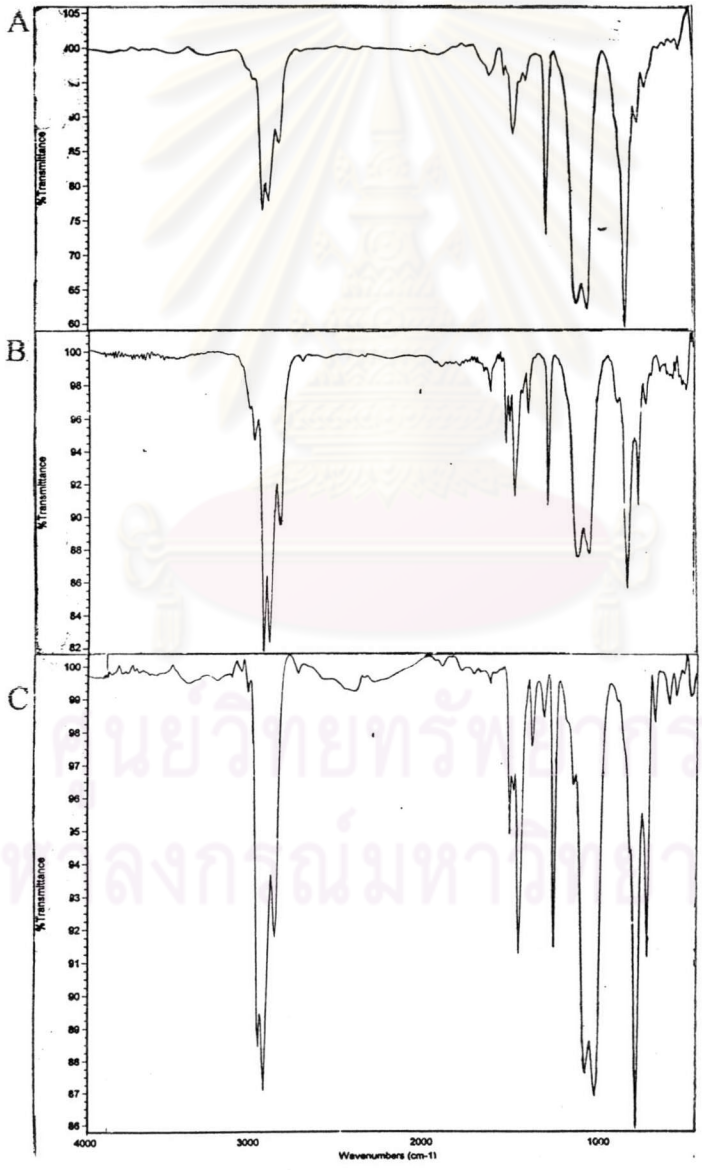

Figure 5.33 FT-IR spectra of the product obtained with (**cpx 1a**)/MAO.
A. $10x10^{-6}$ mol catalyst, Al/Fe 1000, 50°C B. $10x10^{-6}$ mol catalyst, Al/Fe 1000, 30°C
C. $10x10^{-6}$ mol catalyst, Al/Fe 2000, 30°C

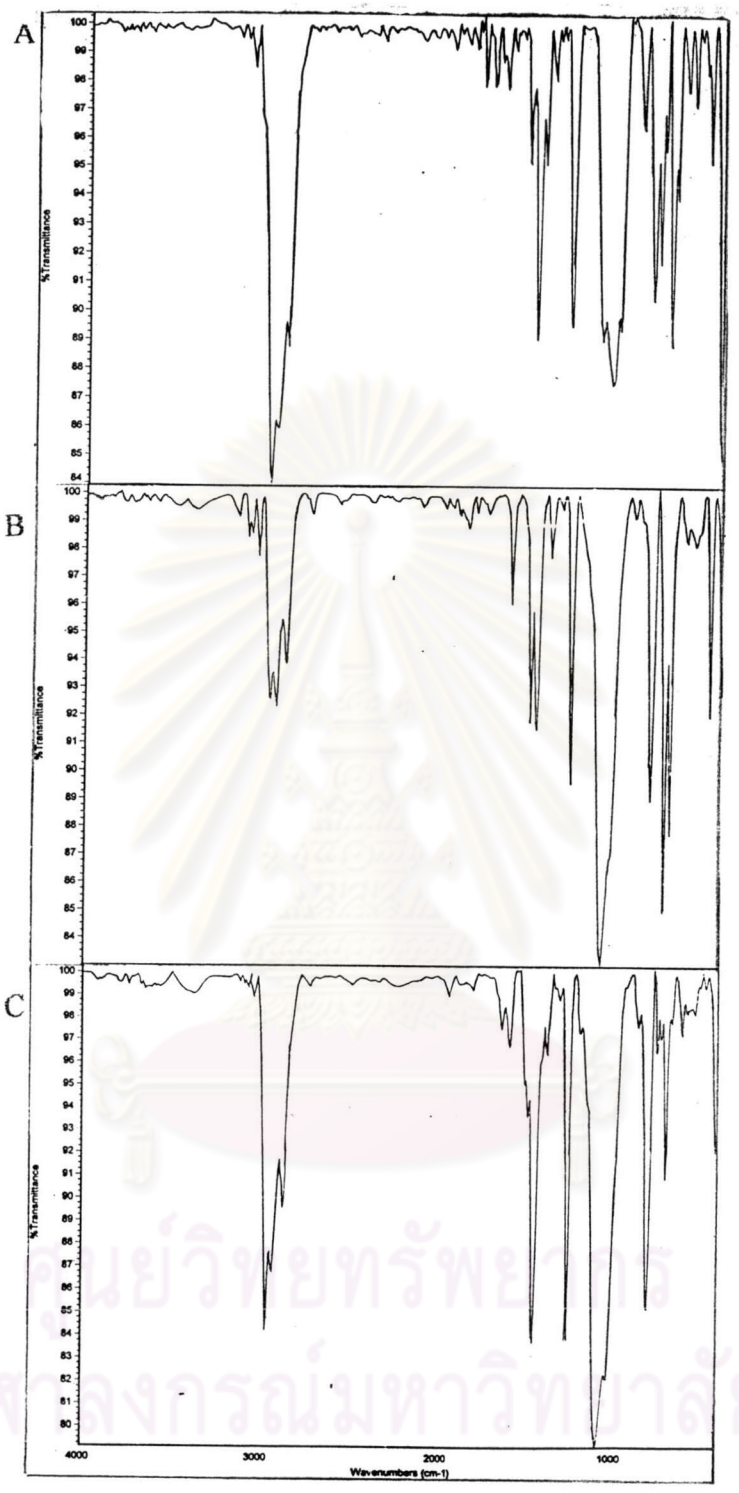

Figure 5.34 FT-IR spectra of the products obtained with (**cpx 1a**)/ $[Ph_3C][B(C_6F_5)_4]$.
A. $10x10^{-6}$ mol catalyst, Al/Fe 200, 30°C B. $10x10^{-6}$ mol catalyst, Al/Fe 200, 0°C
C. $10x10^{-6}$ mol catalyst, Al/Fe 400, 0°C

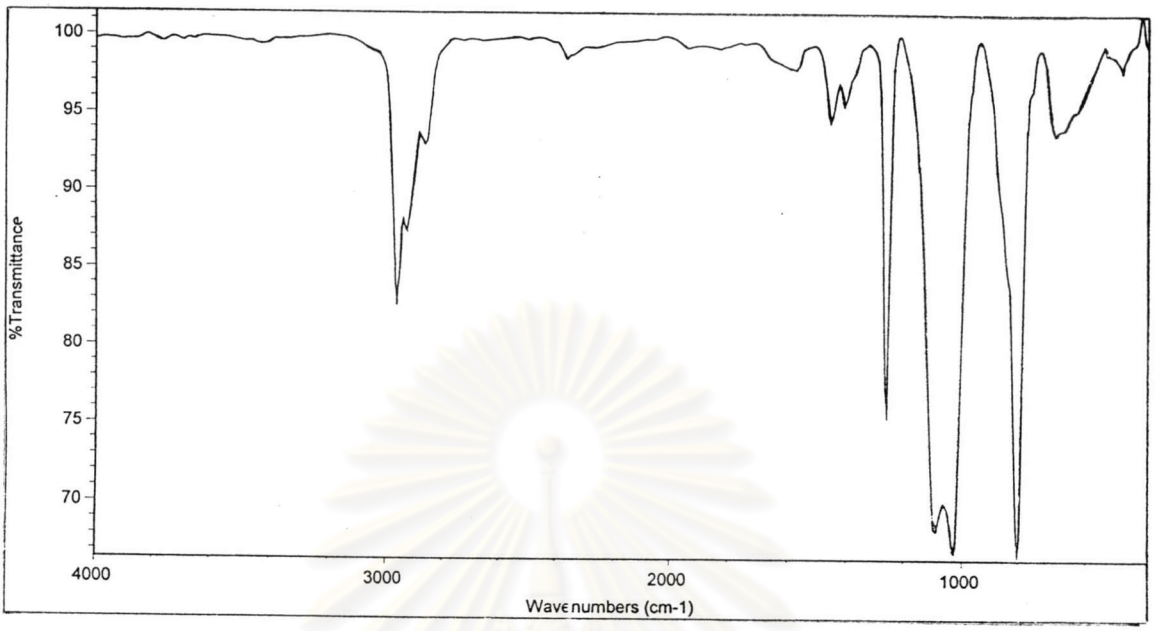

Figure 5.35 FT-IR spectrum of the product obtained with (**cpx 2b**)/$[Ph_3C][B(C_6F_5)_4]$ system ($10.0x10^{-6}$ mol catalyst, Al/Fe mole ratio 200 and T_p 30°C).

Table 5.22. FT-IR data of the product from 1-hexene polymerization by **cpx 1a**/MAO and **cpx 1a**/$[Ph_3C][B(C_6F_5)_4]$

Wave number (cm^{-1})	Ref.[46]	Assignment
2959	2962	asymmetric vibration of saturated end group-CH_3
2856	2850	symmetric vibration of $-CH_2-$
1461	1460	vinylidene end groups
1376	1370	internal double bonds
1200-1000	1200-1000	in-plane bending vibrations of C-H bond
900-800	900-800	out-of-plane bending vibrations of C-H bond

Table 5.23. FT-IR data of the product from 1-hexene polymerization by **cpx 2b** / $[Ph_3C][B(C_6F_5)_4]$

Wave number (cm^{-1})	Ref.[46]	Assignment
2956	2962	asymmetric vibration of saturated end group-CH_3
2856	2850	symmetric vibration of $-CH_2-$
1456	1460	vinylidene end groups
-	1370	internal double bonds
1200-1000	1200-1000	in-plane bending vibrations of C-H bond
900-800	900-800	out-of-plane bending vibrations of C-H bond

From Table 5.22, the strong peaks from 2850 cm^{-1} to 3000 cm^{-1} are due to the vibration of saturated bonds. The resonance peak at 2959 cm^{-1} is assigned to the asymmetric vibration of saturated end group-CH_3. The peak at 2856 is the symmetric vibration of $-CH_2-$. The lower wave number range gives the information on the end groups of the polymers. The signals in range of 1200-1000 are in-plane bending vibration of C-H bond and those at 900-800 cm^{-1} are out-of –plane bending vibration of C-H. There are two kinds of C=C stretching vibrations, a relatively strong vibration at 1461 cm^{-1} corresponding to vinylidene end groups and a weak one at 1376 cm^{-1} corresponding to internal double bonds.

The result from FT-IR in Figures 5.33 and 5.35 showed that there are two types of end group occuring in **cpx 1a** catalyst system; vinylidene end group and internal double bond. β-H elimination resulted in vinylidene end group but internal double bond came from the rearrangement of polymer chain which is then terminated by β-H transfer. Additionally, another termination process that occured was chain transfer to aluminum, resulting in the formation of saturated end group. This result was supported by the polymerization of 1-hexene catalyzed by *rac*-$Me_2Si(1\text{-}C_5H_2\text{-}2\text{-}CH_3\text{-}4\text{-}^tBu)_2Zr$ $(NMe_2)_2$/TIBA/$[Ph_3C][B(C_6F_5)_4]$. The study of this zirconium system found that in the polymerization of 1-hexene monomer, chain termination by β-H elimination resulting in vinylidene end group competed with chain transfer to aluminum.[46] Mechanism of β-H transfer, rearrangement of polymer chain and chain transfer to aluminum was shown in equations 18-20.

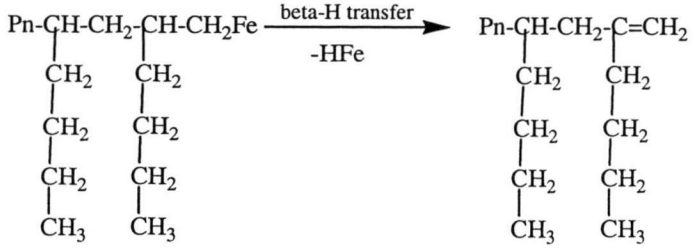

vinylidene end group **(18)**

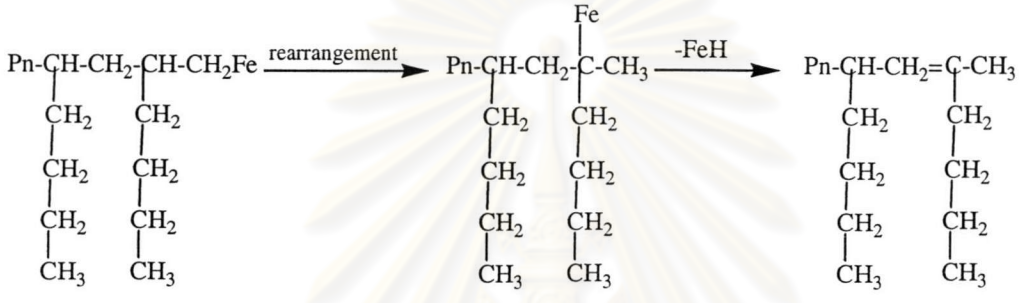

internal double bond **(19)**

saturated end group **(20)**

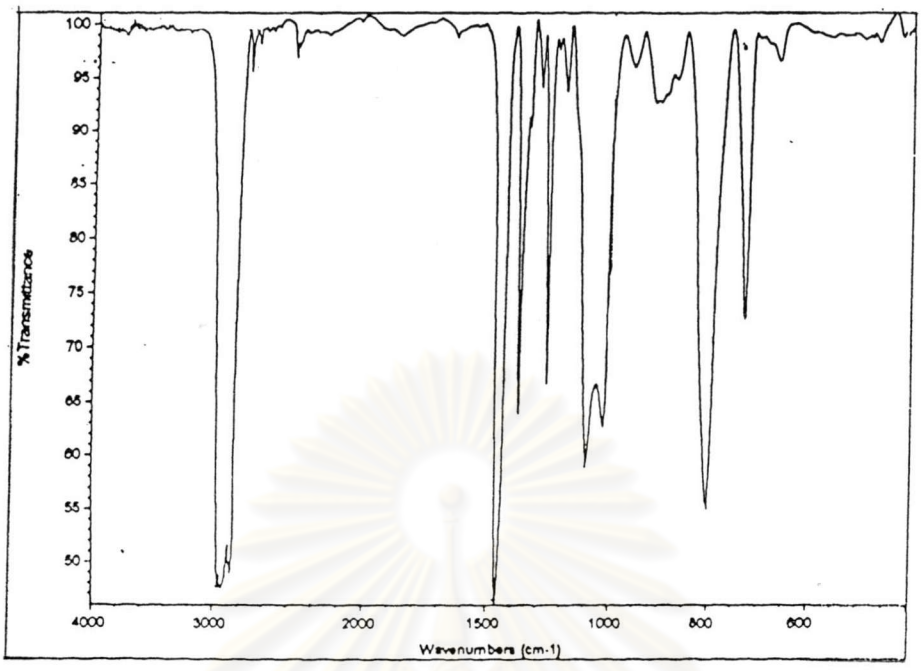

Figure 5.36 FT-IR spectrum of the poly(1-hexene) obtained with *rac*-Et(Ind)$_2$ZrCl$_2$.

Table 5.24. FT-IR data of poly(1-hexene) obtained with *rac*-Et(Ind)$_2$ZrCl$_2$ catalyst

Wave number (cm^{-1})	Ref.[46]	Assignment
2959	2962	asymmetric vibration of saturated end group-CH_3
2856	2850	symmetric vibration of $-CH_2-$
1461	1460	vinylidene end groups
1376	1370	internal double bonds
1200-1000	1200-1000	in-plane bending vibrations of C-H bond
900-800	900-800	out-of-plane bending vibrations of C-H bond

FT-IR in Figure 5.36 showed that there are two types of end group occurring in this zirconium system; vinylidene end group at 1461 cm^{-1} and internal double bond at 1376 cm^{-1}. This result indicated that the termination process should be β-H transfer and rearrangement.

5.3.1.5 Glass transition temperature (T_g)

The glass transition temperature (T_g) of poly(1-hexene) from *rac*-Et(Ind)$_2$$ZrCl_2$/[$PhMe_2NH$][$B(C_6F_5)_4$] system has been determined. DSC curve of the poly(1-hexene) was shown in Figure 5.37.

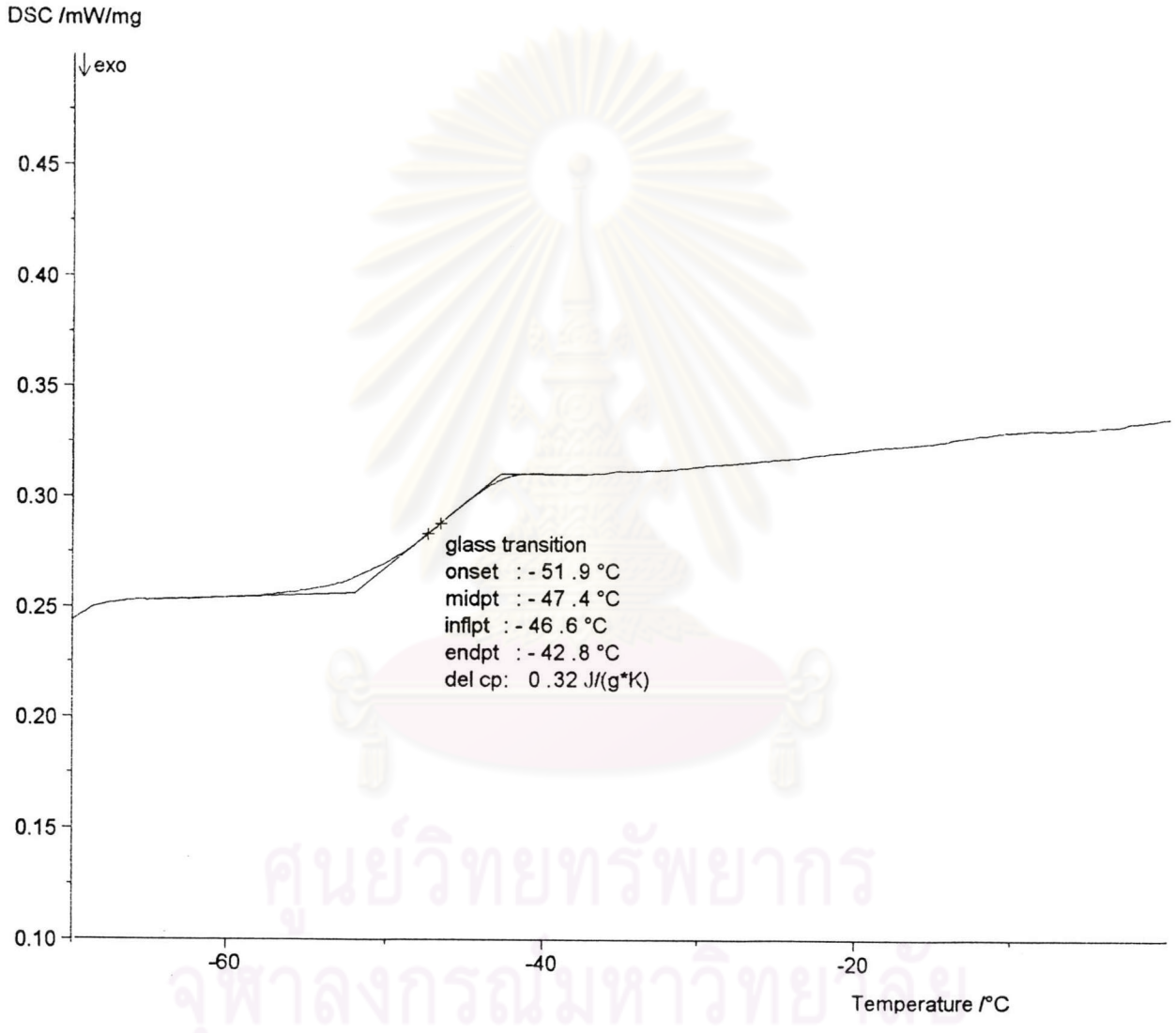

Figure 5.37 DSC curve of poly(1-hexene) produced by *rac*-Et(Ind)$_2$$ZrCl_2$/ [$PhMe_2NH$][$B(C_6F_5)_4$] system.

The glass transition temperature (Tg) was observed at –47°C which was corresponded to the value for isotactic polyhexene. In the cases of **cpx 1a** and **cpx 2b**, products from both catalysts are colorless oil, therefore DSC data was not obtained.

5.3.1.6 Molecular weight (Mw) and molecular weight distribution (MWD)

The molecular weight and molecular weight distribution of poly(1-hexene) produced with *rac*-Et(Ind)$_2$ZrCl$_2$/[PhMe$_2$NH][B(C$_6$F$_5$)$_4$] system was investigated. The polymerization condition was 5.0x10^{-6} mol catalyst, 1 equivalent of boron cocatalsyt, T_p 30°C and Al/Zr mole ratio of 200. The result was shown in Figure 5.38.

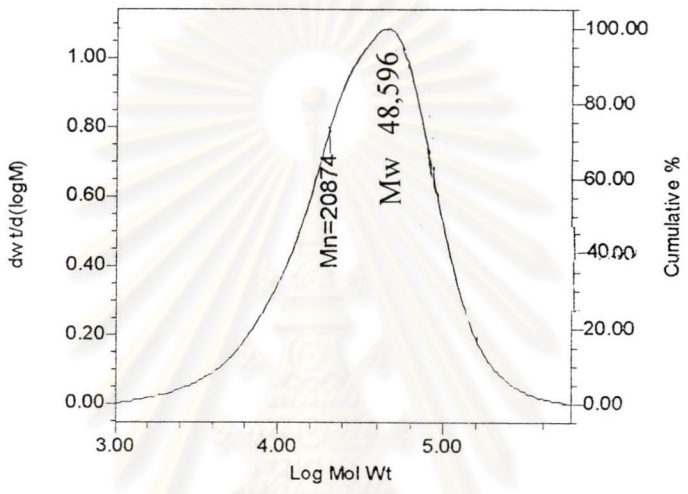

Figure 5.38 GPC curve of poly(1-hexene) from *rac*-Et(Ind)$_2$ZrCl$_2$/ [PhMe$_2$NH][B(C$_6$F$_5$)$_4$] system.

Figure 5.38 showed that this catalyst produced poly(1-hexene) with high molecular weight (Mw 48,596, Mn 20,874) and exhibited molecular weight of 2.33.